Comput. Methods Appl. Mech. Engrg. 198 (2009) 1486–1499

Contents lists available at ScienceDirect

Comput. Methods Appl. Mech. Engrg.

journal homepage: www.elsevier.com/locate/cma

A point interpolation method with least square strain field (PIM-LSS) for solution bounds and ultra-accurate solutions using triangular mesh

X. Xu [a,b,*], G.R. Liu [a,c], G.Y. Zhang [a]

[a] Singapore-MIT Alliance (SMA), E4-04-10, 4 Engineering Drive 3, 117576, Singapore
[b] College of Mathematics, Jilin University, 2699 Qianjin Street, Changchun 130012, PR China
[c] Centre for Advanced Computations in Engineering Science (ACES), Department of Mechanical Engineering, National University of Singapore, 9 Engineering Drive 1, 117576, Singapore

ARTICLE INFO

Article history:
Received 28 July 2008
Received in revised form 16 December 2008
Accepted 22 December 2008
Available online 6 January 2009

Keywords:
Numerical methods
Finite element method
Meshfree method
Point interpolation method
Solution bound
Strain constructed Galerkin weak form
Least square method

ABSTRACT

A point interpolation method with least square strain field (PIM-LSS) is developed for solid mechanics problems using triangular background mesh. In the PIM-LSS, PIM shape functions are used for displacement field construction that may or may not be compatible, and a least square fitting technique is adopted to construct the strain field. A strain constructed Galerkin (SC-Galerkin) weak formulation is then proposed for establishing discretized PIM-LSS models that have a number of special properties. We proved theoretically (1) the PIM-LSS provides a "softening" effect to the FEM model, and a "stiffing" effect to the node-based smoothed point interpolation method (NS-PIM) model; (2) the exact solution is bounded from both by PIM-LSS solutions with strain field of zero-order fitting and that with higher order fitting; (3) There exists a preferred order of fitting for the strain field such that ultra-accurate (one order higher accuracy) solution can be obtained using the PIM-LSS. These theorems and properties have been confirmed in numerical examples.

1. Introduction

To solve engineering problems, many powerful numerical methods have been proposed, such as the Finite Element Methods (FEM) [1–4], Finite Difference Methods [5,6], Finite Volume Methods (FVM) [7,8], and recently Meshfree Methods [9–22].

The FEM is well developed, and is currently the most widely used reliable numerical approach with many commercial software packages available. Most of FEM models are displacement method based on the potential energy principle [1,2], and there are also mixed models based on mixed variational principles [23,24]. The fully compatible displacement FEM usually produces the overestimation of stiffness matrix known as the "overly-stiff" phenomenon, which result in the poor accuracy in the stress of solution especially when the triangular meshes are used [1,2]. In the past several decades, many assumed strain methods have been made in solving these issues in the framework of FEM [25].

On the other hand, meshfree methods offer attractive alternatives to the FEM for many engineering problems, where the treatments on both field function approximation and integration of the weak form are often different from those in the FEM (see, e.g. [20,21]). Some of the nodal integrated meshfree methods based on the standard Galerkin weak form were found spatially unstable, and a strain smoothing technique has been applied by Chen et al. [26] to stabilize the nodal integrated Galerkin meshfree methods. By combining the existing FEM and the strain smoothing technique, Liu et al. proposed the smoothed finite element method (SFEM) that behaves "softer" than the FEM model, and can always produce more accurate solutions [27,28]. The strain smoothing technique was further generalized to allow the use of discontinuous shape functions [22], and such generalized smoothing techniques are used to establish the so-called generalized smoothed Galerkin (GS-Galerkin) weak form. The GS-Galerkin weak form becomes the foundation for the node-based smoothed PIM (or NS-PIM) [29] that is always "softer" than the FEM model of the same mesh, and can usually offer upper bound solutions that are particularly useful in obtaining so-called certified solutions. In addition, an interesting edged-based smoothed PIM (or ES-PIM) [30] has been formulation where the smoothing domains are constructed based on edges of the cells, which can offer a very "close-to-exact" stiffness matrix and works particularly well for triangular cells. These schemes and techniques can obtain solutions of high convergences and high accuracy, and worked very effectively for various problems in science and engineering [31–36].

Recently, some novel schemes of PIM (such as SC-PIM [37] and PIM-CS [38]) by means of constructing the strain fields have

* Corresponding author. Address: College of Mathematics, Jilin University, 2699 Qianjin Street, Changchun 130012, PR China. Tel.: +65 6516 4796; fax: +65 6775 2920.
E-mail addresses: Xuxu@jlu.edu.cn, Smaxx@nus.edu.sg (X. Xu).

0045-7825/$ - see front matter © 2009 Elsevier B.V. All rights reserved.
doi:10.1016/j.cma.2008.12.011

been proposed. In these schemes, the problem domain is divided into triangular cells, over which non-overlapping domains associated with nodes are created. Such a nodal domain is further divided into triangular sub-domains, and the corresponding strain in each sub-domain is constructed by simple linear interpolations using locally smoothed strains at points. These techniques have led some elegant formulations that produce superconvergence solutions for both displacements and strain energy. However, the strain field so-constructed are not smooth but piecewise linear in each nodal domain. Therefore, smoothed strains at quite a number of points are needed to construct the piecewisely linear strain fields, which result in less computational efficiency.

Thus, a question naturally arises: can we construct an analytical and one-piece smooth strain field in each nodal domain? The answer is clearly yes, because we known that strain field constructed in the NS-PIM [29] is one-piece smooth in each nodal domain. However, the strain field is simply constant in the nodal domain, and cannot produce very high accurate solutions even if the higher order displacement models are used [39]. To obtain more accurate solutions, we need to construct a higher order strain field in each nodal domain. Note that a nodal domain usually consists of more sub-domains from different background cells sharing the same node, and corresponding strain field among sub-domains is usually different. If the interpolation method is used to construct the strain field, it will result in much more computational complexity. Naturally, the least square method becomes one of the good candidates.

This work develops a point interpolation method with least square strain field (PIM-LSS): a one-piece smooth strain field in a nodal domain is constructed using the standard least square technique. The present PIM-LSS can constructs a higher order smoothed strain field as desired including the zero-order approximation used in the NS-PIM, and therefore can be considered as a high order extension of the NS-PIM with more general foundation of projection theory. When different order of projection or fitting is used, it is proven that the solution obtained using the PIM-LSS is always between those from FEM and NS-PIM models. Hence, PIM-LSS can be tuned to provide both lower and upper bounds of the exact solution. Furthermore, it is found that there always exists a "best" order of fitting for strain field such that an ultra-accurate solution can be obtained using the PIM-LSS.

The paper is outlined as follows. Section 2 briefs the linear elasticity, and Section 3 gives a briefing on NS-PIM. The idea of the PIM-LSS is formulated in Section 4. The convergence and bound properties of the PIM-LSS are presented and theoretically proven in Sections 5 and 6. In Section 7, numerical examples are presented and discussed to verify the theorems and properties of the PIM-LSS. Conclusions are drawn in Section 8.

2. Brief on basic equations of linearity elasticity [20]

Consider a 2D static elasticity problem governed by the equilibrium equation in the domain Ω bounded by Γ ($\Gamma = \Gamma_u + \Gamma_t$, $\Gamma_u \cap \Gamma_t = 0$) as

$$\mathbf{L}_{\mathrm{d}}^{\mathrm{T}}\boldsymbol{\sigma} + \mathbf{b} = 0 \quad \text{in } \Omega, \tag{1}$$

where $\mathbf{L}_{\mathrm{d}}$ is a matrix of differential operators defined as

$$\mathbf{L}_{\mathrm{d}} = \begin{bmatrix} \frac{\partial}{\partial x_1} & 0 & \frac{\partial}{\partial x_2} \\ 0 & \frac{\partial}{\partial x_2} & \frac{\partial}{\partial x_1} \end{bmatrix}^{\mathrm{T}}, \tag{2}$$

$\boldsymbol{\sigma}^{\mathrm{T}} = (\sigma_{11}, \sigma_{22}, \sigma_{12})$ is the vector of stresses, $\mathbf{b}^{\mathrm{T}} = (b_1, b_2)$ is the vector of body forces.

The stresses relate the strains via the generalized Hook's law:

$$\boldsymbol{\sigma} = \mathbf{D}\boldsymbol{\varepsilon}, \tag{3}$$

where $\mathbf{D}$ is the matrix of material constants [20], and $\boldsymbol{\varepsilon}^{\mathrm{T}} = (\varepsilon_{11}, \varepsilon_{22}, 2\varepsilon_{12})$ is the vector of strains given by

$$\boldsymbol{\varepsilon} = \mathbf{L}_{\mathrm{d}}\mathbf{u}. \tag{4}$$

Essential boundary conditions are:

$$\mathbf{u} = \mathbf{u}_0 \quad \text{on } \Gamma_{\mathbf{u}}, \tag{5}$$

where $\mathbf{u}^{\mathbf{T}} = (u_1, u_2)$ is the vector of the displacement and $\mathbf{u}_0$ is the vector of the prescribed displacements on the essential boundary $\Gamma_{\mathbf{u}}$. In this paper, we consider only homogenous essential boundary conditions $\mathbf{u}_0 = \mathbf{0}$.

Natural boundary conditions are:

$$\mathbf{L}_{\mathrm{n}}^{\mathrm{T}}\boldsymbol{\sigma} = \mathbf{T} \quad \text{on } \Gamma_{\mathbf{t}}, \tag{6}$$

where $\mathbf{T}$ is the vector of the prescribed tractions on the natural boundary Γ_{t}, and $\mathbf{L}_{\mathrm{n}}$ is the matrix of unit outward normal which can be expressed as

$$\mathbf{L}_{\mathrm{n}} = \begin{bmatrix} n_{x_1} & 0 & n_{x_2} \\ 0 & n_{x_2} & n_{x_1} \end{bmatrix}^{\mathrm{T}}. \tag{7}$$

3. Briefing on the NS-PIM [29,39]

In the node-based smoothed PIM (or NS-PIM), the problem domain is first discretized by a set of background triangular cells, as shown in Fig. 1. The displacements in a cell are approximated using PIM shape functions:

$$\bar{\mathbf{u}}(\mathbf{x}) = \sum_{i \in n_e} \boldsymbol{\Phi}_i(\mathbf{x})\bar{\mathbf{d}}_i, \tag{8}$$

where n_e is the set of nodes of the local support domain containing $\mathbf{x}$, $\bar{\mathbf{d}}_i$ is a vector of displacements at this set of nodes, and

$$\boldsymbol{\Phi}_i(\mathbf{x}) = \begin{bmatrix} \psi_i(\mathbf{x}) & 0 \\ 0 & \psi_i(\mathbf{x}) \end{bmatrix} \tag{9}$$

is the matrix of the shape function for node i which are constructed using the PIM procedure and hence is of Delta function property.

In carrying out the numerical integration, the problem domain Ω is divided into smoothing domains Ω_k containing node k, as

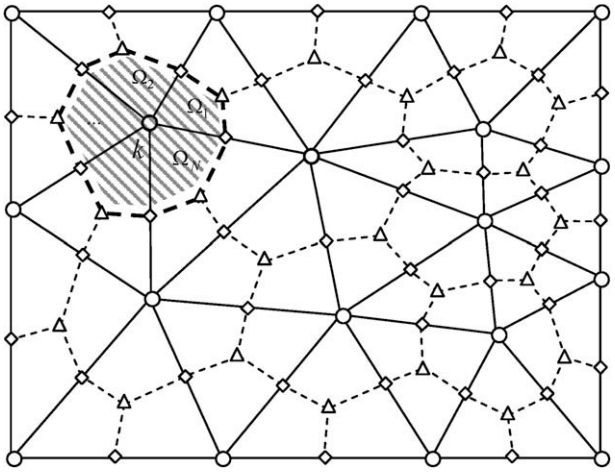

Fig. 1. Triangular elements and the smoothing cells using in NS-PIM.

shown in Fig. 1. The smoothing domain Ω_k is constructed using a triangular element mesh by connecting sequentially the mid-edge-point P to the centroids I of the triangles. The boundary of Ω_k is labeled as Γ_k and the union of all Ω_k forms Ω exactly. NS-PIM uses constant strain for each of the smoothing domains defined by [22]

$$\bar{\boldsymbol{\varepsilon}}_k \equiv \bar{\boldsymbol{\varepsilon}}(\mathbf{x}_k) = \begin{cases} \frac{1}{A_k}\int_{\Omega_k} \tilde{\boldsymbol{\varepsilon}}(\mathbf{x})\,\mathrm{d}\Omega = \frac{1}{A_k}\int_{\Gamma_k} \mathbf{L}_n \bar{\mathbf{u}}\,\mathrm{d}\Gamma & \text{when } \bar{\mathbf{u}} \text{ is continuous in } \Omega_k, \\ \frac{1}{A_k}\int_{\Gamma_k} \mathbf{L}_n \bar{\mathbf{u}}\,\mathrm{d}\Gamma & \text{when } \bar{\mathbf{u}} \text{ is discontinuous in } \Omega_k, \end{cases} \tag{10}$$

where A_k is the area of smoothing domain for node k, and here we assume that $\bar{\mathbf{u}}$ is always continuous on Γ_k.

The Generalized smoothed Galerkin weak form can be written as [22]

$$\int_\Omega \delta\bar{\boldsymbol{\varepsilon}}^{\mathrm{T}}(\bar{\mathbf{u}})\mathbf{D}\bar{\boldsymbol{\varepsilon}}(\bar{\mathbf{u}})\,\mathrm{d}\Omega - \int_\Omega \delta\bar{\mathbf{u}}^{\mathrm{T}}\mathbf{b}\,\mathrm{d}\Omega - \int_{\Gamma_t} \delta\bar{\mathbf{u}}^{\mathrm{T}}\mathbf{T}\,\mathrm{d}\Gamma = 0. \tag{11}$$

Substituting Eq. (10) into Eq. (11) yields the discretized system equation:

$$\bar{\mathbf{K}}\,\bar{\mathbf{d}} = \bar{\mathbf{f}}, \tag{12}$$

where

$$\bar{\mathbf{K}} = \sum_{k=1}^{N} \bar{\mathbf{K}}_{ij}^{(k)} = \sum_{k=1}^{N} \int_{\Omega_k} \bar{\mathbf{B}}_i^{\mathrm{T}}(\mathbf{x}_k)\mathbf{D}\bar{\mathbf{B}}_j^{\mathrm{T}}(\mathbf{x}_k)\mathrm{d}\Omega, \tag{13}$$

$$\bar{\mathbf{f}}_i = \int_{\Gamma_t} \Phi_i \mathbf{T}\,\mathrm{d}\Gamma + \int_\Omega \Phi_i \mathbf{b}\,\mathrm{d}\Omega. \tag{14}$$

4. The idea of the PIM-LSS

4.1. Choice of the shape functions

In the PIM-LSS, the point interpolation method (PIM) is used to construct shape functions using a small set of nodes distributed in a local support domain [20]. Note that background cells have to be used for performing the numerical integration in meshfree methods and the triangular cells that are the most convenient and can be generalized automatically. Therefore, the present PIM-LSS uses the background cells of 3-node triangles for shape functions construction as in the NS-PIM. The details on the construction and detailed distribution of the PIM shape function can be found in Ref. [29]. Using PIM shape functions, the displacement field in the PIM-LSS can be approximated as follows:

$$\hat{\mathbf{u}}(\mathbf{x}) = \sum_{i\in n_e} \mathbf{\Phi}_i(\mathbf{x})\hat{\mathbf{d}}_i, \tag{15}$$

where n_e is the set of nodes in the support domain containing $\mathbf{x}$, $\hat{\mathbf{d}}_i$ is the vector of nodal displacements and $\mathbf{\Phi}_i(\mathbf{x})$ is the matrix of the PIM shape functions for node i as shown in Eq. (9).

The procedure for the shape function construction of PIM-LSS is simple and possesses the following features: (1) it uses local supporting nodes selected based on triangular cells, which overcomes the singular moment matrix issue, and ensures the efficiency in computing PIM shape function; (2) shape functions generated using polynomial basis functions with at least linear terms ensure that the PIM shape functions possess at least linearly consistency; (3) the shape functions are of the Delta function property, which facilitates easy implementation of essential boundary conditions; and (4) this set of shape functions are linearly independent and hence forms a basis for displacement field construction.

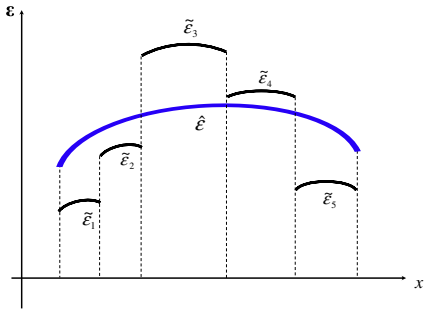

Fig. 2. Reconstructed strain $\hat{\boldsymbol{\varepsilon}}$ and compatible strain $\tilde{\boldsymbol{\varepsilon}}$ in smoothed domain Ω_k. The constructed strain field $\hat{\boldsymbol{\varepsilon}}$ should be proper projection of the compatible strains on a space of lower dimension. Since the compatible strain field is discontinuous, it lives in a space of very high (in fact infinite) dimension. Therefore, a lower order of approximation is always possible.

4.2. Construction for assumed strain field

In the present PIM-LSS, the problem domain Ω is also divided into a set of smoothing domains Ω_k as shown in Fig. 1. Each smoothed domain Ω_k consists of M sub-domains $\Omega_{k,i}$. The strain within $\Omega_{k,i}$ is the compatible strain obtained using Eq. (4). We now construct the smoothed strain using the least square technique [40,41]. By minimizing the sum of squared deviations, PIM-LSS constructs a strain field that is one-piece and smooth in the nodal domain Ω_k (see Fig. 2).

Consider now the assumed displacement field is continuous, and hence the compatible strain $\tilde{\boldsymbol{\varepsilon}}$ is defined in the problem domain. Let $\{\varphi_i\}_{i=1}^n$ be an independent sequence of functions that can be used as a basis for strain field construction. We can then construct a strain field based upon the compatible strain $\tilde{\boldsymbol{\varepsilon}}$ using a linear combination of the basis functions $\{\varphi_i\}_{i=1}^n$

$$\hat{\boldsymbol{\varepsilon}} = \sum_{i=1}^{n} \mathbf{a}_i \varphi_i \tag{16}$$

with the coefficients $(\mathbf{a}_1, \mathbf{a}_2, \ldots, \mathbf{a}_n)$ to be determined such that

$$\delta(\mathbf{a}_1, \mathbf{a}_2, \ldots, \mathbf{a}_n) \equiv (\hat{\boldsymbol{\varepsilon}} - \tilde{\boldsymbol{\varepsilon}}, \mathbf{D}(\hat{\boldsymbol{\varepsilon}} - \tilde{\boldsymbol{\varepsilon}})) \tag{17}$$

is minimized, where $\hat{\boldsymbol{\varepsilon}} = (\hat{\varepsilon}_{11}, \hat{\varepsilon}_{22}, \hat{\varepsilon}_{12})^{\mathrm{T}}$, $\mathbf{a}_i = (a_{11}^i, a_{22}^i, a_{12}^i)^{\mathrm{T}}$.

In Eq. (17), the inner produce $(\cdot,\cdot)$ of vector functions $\mathbf{f}$ and $\mathbf{g}$ is defined by

$$(\mathbf{f}, \mathbf{g}) = \int_\Omega \mathbf{f}^{\mathrm{T}}\mathbf{g}\,\mathrm{d}\Omega \tag{18}$$

and the norm of $\mathbf{f}$ is defined by

$$\|\mathbf{f}\| = \left[\int_\Omega \mathbf{f}^{\mathrm{T}}\mathbf{f}\,\mathrm{d}\Omega\right]^{1/2}. \tag{19}$$

Note that error function (17) is a little different from that in standard least square method defined by $(\hat{\boldsymbol{\varepsilon}} - \tilde{\boldsymbol{\varepsilon}}, \hat{\boldsymbol{\varepsilon}} - \tilde{\boldsymbol{\varepsilon}})$, due to the introduction of $\mathbf{D}$ in the formulation. However, because of the positivity of elasticity constant matrix $\mathbf{D}$, the error function δ is still a quadratic function of the variables $\mathbf{a}_i$, and hence has always one minimum. Therefore, the procedure for calculating coefficient $\mathbf{a}_i$ in PIM-LSS is similar to that in the standard least square method.

Note both the constructed strain $\hat{\boldsymbol{\varepsilon}}$ and the compatible strain $\tilde{\boldsymbol{\varepsilon}}$ are piecewise integral in entire problem domain. Substituting Eq. (16) into (17) gives

$$\begin{aligned} \delta &= (\hat{\boldsymbol{\varepsilon}} - \tilde{\boldsymbol{\varepsilon}}, \mathbf{D}(\hat{\boldsymbol{\varepsilon}} - \tilde{\boldsymbol{\varepsilon}})) = (\hat{\boldsymbol{\varepsilon}}, \mathbf{D}\hat{\boldsymbol{\varepsilon}}) - 2(\hat{\boldsymbol{\varepsilon}}, \mathbf{D}\tilde{\boldsymbol{\varepsilon}}) + (\tilde{\boldsymbol{\varepsilon}}, \mathbf{D}\tilde{\boldsymbol{\varepsilon}}) \\ &= \left(\sum_{i=1}^{n} \mathbf{a}_i\varphi_i, \mathbf{D}\sum_{r=1}^{n} \mathbf{a}_r\varphi_r\right) - 2\left(\sum_{i=1}^{n} \mathbf{a}_i\varphi_i, \mathbf{D}\tilde{\boldsymbol{\varepsilon}}\right) + (\tilde{\boldsymbol{\varepsilon}}, \mathbf{D}\tilde{\boldsymbol{\varepsilon}}) \end{aligned} \tag{20}$$

and

$$\frac{\partial\delta}{\partial\mathbf{a}_j} = \left(\varphi_j\mathbf{J}, \mathbf{D}\sum_{i=1}^{n}\mathbf{a}_i\varphi_i\right) + \left(\sum_{i=1}^{n}\mathbf{a}_i\varphi_i, \mathbf{D}\varphi_j\mathbf{J}\right) - 2(\varphi_j\mathbf{J}, \mathbf{D}\tilde{\boldsymbol{\varepsilon}})$$
$$= 2\sum_{i=1}^{n}(\varphi_j\mathbf{J}, \mathbf{D}\mathbf{a}_i\varphi_i) - 2(\varphi_j\mathbf{J}, \mathbf{D}\tilde{\boldsymbol{\varepsilon}})$$
$$= 2\left(\varphi_j\mathbf{J}, \mathbf{D}\left(\sum_{i=1}^{n}\mathbf{a}_i\varphi_i - \tilde{\boldsymbol{\varepsilon}}\right)\right) = 2(\varphi_j\mathbf{J}, \mathbf{D}(\hat{\boldsymbol{\varepsilon}} - \tilde{\boldsymbol{\varepsilon}}))$$
$$= 2\sum_{i=1}^{n}(\varphi_j\mathbf{J}, \mathbf{D}\varphi_i)\mathbf{a}_i - 2(\varphi_j\mathbf{J}, \mathbf{D}\tilde{\boldsymbol{\varepsilon}})), \tag{21}$$

where, $\mathbf{J}$ is the 3rd order identity matrix. Hence, the minimum of δ must satisfy

$$\frac{\partial\delta}{\partial\mathbf{a}_j} = 0, \quad j = 1, 2, \ldots, n. \tag{22}$$

Substituting Eq. (21) into (22) yields

$$\sum_{i=1}^{n}(\varphi_j\mathbf{J}, \mathbf{D}\varphi_i)\mathbf{a}_i - (\varphi_j\mathbf{J}, \mathbf{D}\tilde{\boldsymbol{\varepsilon}})) = 0, \quad j = 1, 2, \ldots, n. \tag{23}$$

For the isotropic elastic materials, by direct computation, we know that the solutions of Eq. (23) is exactly same as the solution of the following equation:

$$\sum_{i=1}^{n}(\varphi_j, \varphi_i)\mathbf{a}_i = (\varphi_j\mathbf{J}, \tilde{\boldsymbol{\varepsilon}})), \quad j = 1, 2, \ldots, n. \tag{24}$$

Therefore, when function sequence $\{\varphi_i\}_{i=1}^{n}$ is independent, Eq. (24) has an unique solution $\{\mathbf{a}_i\}_{i=1}^{n}$ which is termed as the least-square approximation to compatible strain over the basis $\{\varphi_i\}_{i=1}^{n}$.

In actual computation, it is not easy to obtain the solution of Eq. (24), especially when higher order fittings are used [40,41]. Therefore, Gram–Schmidt orthogonalization procedure [42] is usually used to simplify computation. Assume the space W is spanned by the vectors $\{\varphi_i\}_{i=1}^{n}$, which are not necessarily orthogonal. An orthogonal set of vector $\{\Phi_i\}_{i=1}^{n}$ can be obtained by the following steps:

1. Normalize φ_1 by setting $\Phi_1 = \varphi_1/\|\varphi_1\|$;
2. Find the projection of φ_2 in the directions of Φ_1, that is $(\varphi_2,\Phi_1)\Phi_1$;
3. Subtract the projection of φ_2 on Φ_1 from φ_2 and normalize the result:

$$\Phi_2 = \frac{z_2}{\|z_2\|}, \quad \text{where } z_2 = \varphi_2 - (\varphi_2, \Phi_1)\Phi_1; \tag{25}$$

4. For the nth vector

$$\Phi_n = \frac{z_n}{\|z_n\|} \quad \text{where } z_n = \varphi_n - \sum_{i=1}^{n-1}(\varphi_n, \Phi_i)\Phi_i; \tag{26}$$

5. Let the vector $y = \varphi_{n+1}$ where space V is spanned by $\{\Phi_i\}_{i=1}^{n+1}$. Then the next vector is given by

$$z_{n+1} = y - \sum_{i=1}^{n-1}(y, \Phi_i)\Phi_i. \tag{27}$$

Note that z_{n+1} is orthogonal to Φ_i for $i \leqslant n$.

Therefore, the best approximation of compatible strain is

$$\hat{\boldsymbol{\varepsilon}} = \sum_{i=1}^{n}(\Phi_i\mathbf{J}, \tilde{\boldsymbol{\varepsilon}})\Phi_i. \tag{28}$$

The overall procedure of strain field construction in the PIM-LSS is as follows. The displacement at any point in a background cell is first approximated via point interpolation using Eq. (15). The strains within each of domains Ω_k are next constructed using Eqs. (16) and (23). Therefore, the strain depends entirely on the assumed displacement field, and no additional degrees of freedoms are introduced. Furthermore, the dimension of the discretized system equation in our PIM-LSS model will be exactly the same as the FEM model of the same mesh.

5. Weak form for PIM-LSS

To formulate PIM-LSS, we construct a strain constructed Galerkin (or SC-Galerkin) functional for variational formulation as follows:

$$\Pi(\mathbf{v}) = \int_\Omega \frac{1}{2}\hat{\boldsymbol{\varepsilon}}^{\mathbf{T}}(\mathbf{v})\mathbf{D}\hat{\boldsymbol{\varepsilon}}(\mathbf{v})\Omega - \int_\Omega \mathbf{v}^{\mathrm{T}}\mathbf{b}\,\mathrm{d}\Omega - \int_{\Gamma_t}\mathbf{v}^{\mathrm{T}}\mathbf{T}\,\mathrm{d}\Gamma. \tag{29}$$

Note that displacement $\mathbf{v}$ is the only unknown field in Eq. (29).

The stationary condition of Eq. (29) is

$$\delta\Pi(\mathbf{v}) = \int_\Omega \delta\hat{\boldsymbol{\varepsilon}}^{\mathbf{T}}(\mathbf{v})\mathbf{D}\hat{\boldsymbol{\varepsilon}}(\mathbf{v})\Omega - \int_\Omega \delta\mathbf{v}^{\mathrm{T}}\mathbf{b}\,\mathrm{d}\Omega - \int_{\Gamma_t}\delta\mathbf{v}^{\mathrm{T}}\mathbf{T}\,\mathrm{d}\Gamma = 0. \tag{30}$$

Substituting Eq. (16) into (30) leads to the discretized system equations as follows:

$$\widehat{\mathbf{K}}\hat{\mathbf{d}} = \hat{\mathbf{f}}, \tag{31}$$

where $\widehat{\mathbf{K}}$ is the stiffness matrix, and

$$\hat{\mathbf{f}} = -\int_\Omega \boldsymbol{\Phi}^{\mathrm{T}}\mathbf{b}\,\mathrm{d}\Omega + \int_{\Gamma_t}\boldsymbol{\Phi}^{\mathrm{T}}\mathbf{T}\,\mathrm{d}\Gamma. \tag{32}$$

Theorem 1 (Convergence theorem). *The PIM-LSS based on Eq. (29) is variationally consistent; and the solution obtained converges to the exact solution of original strong form when the dimension of all the cells approaches to zero, if the assumed displacement is continuous over the problem domain.*

Proof. When the assumed displacement is continuous over the problem domain, from Section 4, we know that the constructed strain field represents a mean value of the compatible strain in nodal domain Ω_k in the least square. The constructed strain field depends only on the assumed displacement field. Therefore, displacement field is the only unknown field, and there is no increase of unknown variables compared to the standard Galerkin formulation.

Substituting $\hat{\boldsymbol{\varepsilon}}(\mathbf{v})$ into the Hellinger–Reissner's two-field energy functional [23–25], we have

$$\Pi(\mathbf{v}) = \int_\Omega -\frac{1}{2}\hat{\boldsymbol{\varepsilon}}^{\mathbf{T}}(\mathbf{v})\mathbf{D}\hat{\boldsymbol{\varepsilon}}(\mathbf{v})\Omega + \int_\Omega \hat{\boldsymbol{\varepsilon}}^{\mathrm{T}}(\mathbf{v})\mathbf{D}(\mathbf{L}_{\mathrm{d}}\mathbf{v})\mathrm{d}\Omega$$
$$- \int_\Omega \mathbf{v}^{\mathrm{T}}\mathbf{b}\,\mathrm{d}\Omega - \int_{\Gamma_t}\mathbf{v}^{\mathrm{T}}\mathbf{T}\,\mathrm{d}\Gamma. \tag{33}$$

On the other hand, from (21) and (22), we can obtain

$$(\varphi_j\mathbf{J}, \mathbf{D}(\hat{\boldsymbol{\varepsilon}} - \tilde{\boldsymbol{\varepsilon}})) = 0, \quad \text{for all } j = 1, 2, \ldots, n. \tag{34}$$

From (34), we have

$$\left(\sum_{j=1}^{n}\mathbf{a}_j\varphi_j, \mathbf{D}(\hat{\boldsymbol{\varepsilon}} - \tilde{\boldsymbol{\varepsilon}})\right) = 0 \tag{35}$$

or

$$(\hat{\boldsymbol{\varepsilon}}, \mathbf{D}(\hat{\boldsymbol{\varepsilon}} - \tilde{\boldsymbol{\varepsilon}})) = 0, \tag{36}$$

where $\{\mathbf{a}_j\}_{j=1}^{n}$ is obtained from Eq. (23).

Eq. (36) can be written as

$$\int_\Omega \hat{\boldsymbol{\varepsilon}}^{\mathrm{T}}\mathbf{D}\hat{\boldsymbol{\varepsilon}}\,\mathrm{d}\Omega = \int_\Omega \hat{\boldsymbol{\varepsilon}}^{\mathrm{T}}\mathbf{D}\tilde{\boldsymbol{\varepsilon}}\,\mathrm{d}\Omega, \tag{37}$$

which is the orthogonal condition required for variational consistence [43]. Therefore, the PIM-LSS is variationally consistent, and the substitution Eq. (37) into (33) leads to the energy functional (29) for PIM-LSS.

In addition, it is well known that for any assumed strain field the numerical solution obtained from the Hellinger–Reissner's two-field variational principle converges to real solution of original strong form [23–25], as long as the stability of the discrete model is ensured. Now, based on the analysis given in [22,44], we know that the node-based smoothing domains are linearly independent [44] and satisfy the minimum number of smoothing domains [22]. Therefore, the PIM-LSS will be stable. Therefore, the solution obtained using the PIM-LSS based on (29) also converges to the real solution of original strong form. This completes the proof. □

We have the following corollary.

Corollary 1. *The stiffness matrix* $\widehat{\mathbf{K}}$ *obtained using PIM-LSS is symmetric, positive definite and has the same dimensions as that of FEM when the same mesh is used.*

Note that Theorem 1 has condition that the assumed displacement is continuous over the problem domain. When PIM shape function is not continuous, the proof of the convergence theorem needs to be performed based on the *G* space theory [44].

6. Bound property of strain energy potential for the PIM-LSS

Theorem 2 (Projection theorem). *Suppose the compatible strain vector* $\tilde{\boldsymbol{\varepsilon}}$ *exists in the problem domain and is in a finite dimensional space S; strain vector* $\hat{\boldsymbol{\varepsilon}}$ *obtained using the PIM-LSS is in the subspace W of S spanned by* $\varphi_1, \varphi_2, \ldots, \varphi_n$. *Then we have*

$$(\tilde{\boldsymbol{\varepsilon}} - \hat{\boldsymbol{\varepsilon}}, \mathbf{D}\boldsymbol{\varepsilon}') = 0 \quad \forall \boldsymbol{\varepsilon}' \in W, \tag{38}$$

$$(\tilde{\boldsymbol{\varepsilon}} - \hat{\boldsymbol{\varepsilon}}, \mathbf{D}(\tilde{\boldsymbol{\varepsilon}} - \hat{\boldsymbol{\varepsilon}})) = \inf_{\boldsymbol{\varepsilon}' \in W} (\tilde{\boldsymbol{\varepsilon}} - \boldsymbol{\varepsilon}', \mathbf{D}(\tilde{\boldsymbol{\varepsilon}} - \boldsymbol{\varepsilon}')), \tag{39}$$

which means that the constructed strain field is a "best" projection from the compatible strain field.

Proof. From Section 4, we know that any strain vector in space *W* can be represented as

$$\boldsymbol{\varepsilon}' = \sum_{i=1}^{n} \mathbf{b}_i \varphi_i, \tag{40}$$

where not all the vector $\mathbf{b}_i$ ($i = 1,2,\ldots,n$) is zero vector.

In addition, from Eqs. (21) and (22), we have

$$(\varphi_j \mathbf{J}, \mathbf{D}(\tilde{\boldsymbol{\varepsilon}} - \hat{\boldsymbol{\varepsilon}})) = 0 \quad \text{for all } j = 1, 2, \ldots, n, \tag{41}$$

which indicates that

$$\left(\sum_{j=1}^{n} \mathbf{b}_j \varphi_j, \mathbf{D}(\tilde{\boldsymbol{\varepsilon}} - \hat{\boldsymbol{\varepsilon}})\right) = 0 \tag{42}$$

or

$$(\tilde{\boldsymbol{\varepsilon}} - \hat{\boldsymbol{\varepsilon}}, \mathbf{D}\boldsymbol{\varepsilon}') = 0. \tag{43}$$

On the other hand, for any $\varepsilon' \in W$ we have

$$\begin{aligned}(\tilde{\boldsymbol{\varepsilon}} - \boldsymbol{\varepsilon}', \mathbf{D}(\tilde{\boldsymbol{\varepsilon}} - \boldsymbol{\varepsilon}')) &= (\tilde{\boldsymbol{\varepsilon}} - \hat{\boldsymbol{\varepsilon}} + \hat{\boldsymbol{\varepsilon}} - \boldsymbol{\varepsilon}', \mathbf{D}(\tilde{\boldsymbol{\varepsilon}} - \hat{\boldsymbol{\varepsilon}} + \hat{\boldsymbol{\varepsilon}} - \boldsymbol{\varepsilon}')) \\ &= (\tilde{\boldsymbol{\varepsilon}} - \hat{\boldsymbol{\varepsilon}}, \mathbf{D}(\tilde{\boldsymbol{\varepsilon}} - \hat{\boldsymbol{\varepsilon}})) + 2(\tilde{\boldsymbol{\varepsilon}} - \hat{\boldsymbol{\varepsilon}}, \mathbf{D}(\hat{\boldsymbol{\varepsilon}} - \boldsymbol{\varepsilon}')) + (\hat{\boldsymbol{\varepsilon}} \\ &\quad - \boldsymbol{\varepsilon}', \mathbf{D}(\hat{\boldsymbol{\varepsilon}} - \boldsymbol{\varepsilon}')).\end{aligned} \tag{44}$$

Note that $\boldsymbol{\varepsilon}' - \hat{\boldsymbol{\varepsilon}} \in W$, and thus $(\tilde{\boldsymbol{\varepsilon}} - \hat{\boldsymbol{\varepsilon}}, \mathbf{D}(\hat{\boldsymbol{\varepsilon}} - \boldsymbol{\varepsilon}')) = 0$ from Eq. (38). Therefore, according to the positivity of elasticity constant matrix **D**, we have

$$\begin{aligned}(\tilde{\boldsymbol{\varepsilon}} - \boldsymbol{\varepsilon}', \mathbf{D}(\tilde{\boldsymbol{\varepsilon}} - \boldsymbol{\varepsilon}')) &= (\tilde{\boldsymbol{\varepsilon}} - \hat{\boldsymbol{\varepsilon}}, \mathbf{D}(\tilde{\boldsymbol{\varepsilon}} - \hat{\boldsymbol{\varepsilon}})) + (\hat{\boldsymbol{\varepsilon}} - \boldsymbol{\varepsilon}', \mathbf{D}(\hat{\boldsymbol{\varepsilon}} - \boldsymbol{\varepsilon}')) \\ &\geqslant (\tilde{\boldsymbol{\varepsilon}} - \hat{\boldsymbol{\varepsilon}}, \mathbf{D}(\tilde{\boldsymbol{\varepsilon}} - \hat{\boldsymbol{\varepsilon}}))\end{aligned} \tag{45}$$

or

$$\|\tilde{\boldsymbol{\varepsilon}} - \hat{\boldsymbol{\varepsilon}}\| \leqslant \|\tilde{\boldsymbol{\varepsilon}} - \boldsymbol{\varepsilon}'\| \quad \forall \boldsymbol{\varepsilon}' \in W. \tag{46}$$

In Eq. (46), "=" stands if and only if $\boldsymbol{\varepsilon}' = \hat{\boldsymbol{\varepsilon}}$. Therefore, we have

$$(\tilde{\boldsymbol{\varepsilon}} - \hat{\boldsymbol{\varepsilon}}, \mathbf{D}(\tilde{\boldsymbol{\varepsilon}} - \hat{\boldsymbol{\varepsilon}})) = \inf_{\boldsymbol{\varepsilon}' \in W} (\tilde{\boldsymbol{\varepsilon}} - \boldsymbol{\varepsilon}', \mathbf{D}(\tilde{\boldsymbol{\varepsilon}} - \boldsymbol{\varepsilon}')). \tag{47}$$

This completes the proof. □

A simple geometric interpretation to Theorem 2 is as follows.

Consider a compatible strain vector $\tilde{\boldsymbol{\varepsilon}}$ in space *S*, and the subspace *W* of *S* spanned by $\varphi_1, \varphi_2, \ldots, \varphi_n$. Of course, if $\tilde{\boldsymbol{\varepsilon}}$ lies in *W*, the solution is trivial. Generally, compatible strain vector $\tilde{\boldsymbol{\varepsilon}}$ is not in *W*. An important question is that which vector $\hat{\boldsymbol{\varepsilon}}$ in *W* "best" approximates $\tilde{\boldsymbol{\varepsilon}}$. One definition of "best" is that the energy error norm $(\hat{\boldsymbol{\varepsilon}} - \tilde{\boldsymbol{\varepsilon}}, \mathbf{D}(\hat{\boldsymbol{\varepsilon}} - \tilde{\boldsymbol{\varepsilon}}))$ is a minimum. It is clear from Fig. 3 that the error norm is minimized when $\hat{\boldsymbol{\varepsilon}}$ is the projection of $\tilde{\boldsymbol{\varepsilon}}$ onto *W* in a direction perpendicular to *W*. Since $(\hat{\boldsymbol{\varepsilon}} - \tilde{\boldsymbol{\varepsilon}}, \mathbf{D}(\hat{\boldsymbol{\varepsilon}} - \tilde{\boldsymbol{\varepsilon}}))$ involves squaring the length of the vector $\tilde{\boldsymbol{\varepsilon}}$, minimizing the norm of the error vector is referred to as a least square error criterion. Therefore, strain $\hat{\boldsymbol{\varepsilon}}$ is the projection of $\tilde{\boldsymbol{\varepsilon}}$ (in the meaning of energy norm) onto the subspace *W* spanned by $\varphi_1, \varphi_2, \ldots, \varphi_n$.

Theorem 3 (Bound theorem). *For any given continuous displacement field* **v**, *if the strain field is obtained using Eqs. (16) and (23), and discretized system equations is provided by* Eqs. (29)–(32), *we then have*

$$\widehat{U}(\mathbf{v}) \leqslant \widetilde{U}(\mathbf{v}), \tag{48}$$

where, $\widehat{U}(\mathbf{v})$ is the strain energy obtained using the PIM-LSS given by

$$\widehat{U}(\mathbf{v}) = \frac{1}{2}\int_\Omega \hat{\boldsymbol{\varepsilon}}^{\mathrm{T}}(\mathbf{v})\mathbf{D}\hat{\boldsymbol{\varepsilon}}(\mathbf{v})\,\mathrm{d}\Omega, \tag{49}$$

$\widetilde{U}(\mathbf{v})$ is that using the FEM given by

$$\widetilde{U}(\mathbf{v}) = \frac{1}{2}\int_\Omega \tilde{\boldsymbol{\varepsilon}}^{\mathrm{T}}(\mathbf{v})\mathbf{D}\tilde{\boldsymbol{\varepsilon}}(\mathbf{v})\,\mathrm{d}\Omega. \tag{50}$$

Proof. Using Eq. (36) and the positivity of **D**, we can easily obtain that

$$\begin{aligned}(\hat{\boldsymbol{\varepsilon}} - \tilde{\boldsymbol{\varepsilon}}, \mathbf{D}(\hat{\boldsymbol{\varepsilon}} - \tilde{\boldsymbol{\varepsilon}})) &= (\hat{\boldsymbol{\varepsilon}}, \mathbf{D}\hat{\boldsymbol{\varepsilon}}) - 2(\hat{\boldsymbol{\varepsilon}}, \mathbf{D}\tilde{\boldsymbol{\varepsilon}}) + (\tilde{\boldsymbol{\varepsilon}}, \mathbf{D}\tilde{\boldsymbol{\varepsilon}}) \\ &= (\hat{\boldsymbol{\varepsilon}}, \mathbf{D}\hat{\boldsymbol{\varepsilon}}) - 2(\hat{\boldsymbol{\varepsilon}}, \mathbf{D}\hat{\boldsymbol{\varepsilon}}) + (\tilde{\boldsymbol{\varepsilon}}, \mathbf{D}\tilde{\boldsymbol{\varepsilon}}) \\ &= (\tilde{\boldsymbol{\varepsilon}}, \mathbf{D}\tilde{\boldsymbol{\varepsilon}}) - (\hat{\boldsymbol{\varepsilon}}, \mathbf{D}\hat{\boldsymbol{\varepsilon}}) \geqslant 0\end{aligned} \tag{51}$$

or

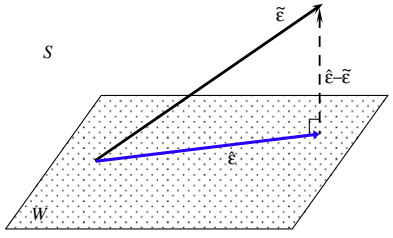

Fig. 3. Strain $\hat{\boldsymbol{\varepsilon}}$ obtained using the least square procedure is an orthogonal projector of $\tilde{\boldsymbol{\varepsilon}}$ onto the subspace W spanned by $\varphi_1, \varphi_2, \ldots, \varphi_n$. It is a "best" approximation to $\tilde{\boldsymbol{\varepsilon}}$ in sub-space *W* in the meaning of energy norm.

$$(\hat{\boldsymbol{\varepsilon}}, \mathbf{D}\hat{\boldsymbol{\varepsilon}}) \leqslant (\tilde{\boldsymbol{\varepsilon}}, \mathbf{D}\tilde{\boldsymbol{\varepsilon}}), \tag{52}$$

which completes the proof. □

Theorem 4. *When the same set of shape functions is used, the strain energy obtained from the PIM-LSS solution is no-less than that from the FEM solution based on a fully compatible model:*

$$\frac{1}{2}\hat{\mathbf{d}}^{\mathrm{T}}\widehat{\mathbf{K}}\hat{\mathbf{d}} \geqslant \frac{1}{2}\tilde{\mathbf{d}}^{\mathrm{T}}\widetilde{\mathbf{K}}\tilde{\mathbf{d}}. \tag{53}$$

Proof. Eq. (48) can be written in discrete form of arbitrary nodal displacement $\mathbf{d}$ as

$$\frac{1}{2}\mathbf{d}^{\mathrm{T}}\widehat{\mathbf{K}}\mathbf{d} \leqslant \frac{1}{2}\mathbf{d}^{\mathrm{T}}\widetilde{\mathbf{K}}\mathbf{d}. \tag{54}$$

Therefore, it is clear that

$$\frac{1}{2}\mathbf{d}^{\mathrm{T}}(\widetilde{\mathbf{K}} - \widehat{\mathbf{K}})\mathbf{d} \geqslant 0, \tag{55}$$

which indicates that matrix $(\widetilde{\mathbf{K}} - \widehat{\mathbf{K}})$ is semi-positive definite. In mechanics, it implies that $\widehat{\mathbf{K}}$ is "softer" that $\widetilde{\mathbf{K}}$. In addition, the discrete solutions of FEM and PIM-LSS at their stationary points can be written as

$$\tilde{\mathbf{d}} = \widetilde{\mathbf{K}}^{-1}\mathbf{f}, \quad \hat{\mathbf{d}} = \widehat{\mathbf{K}}^{-1}\mathbf{f}, \tag{56}$$

where $\mathbf{f}$ is commonly defined by Eq. (32).

As the stiffness matrix $\widehat{\mathbf{K}}$ and $\widetilde{\mathbf{K}}$ are symmetric, at the stationary point we have the total energy as follows:

$$\begin{cases} \tilde{\Pi}(\tilde{\mathbf{d}}) = \frac{1}{2}\tilde{\mathbf{d}}^{\mathrm{T}}\widetilde{\mathbf{K}}\tilde{\mathbf{d}} - \tilde{\mathbf{d}}^{\mathrm{T}}\mathbf{f} = -\frac{1}{2}\tilde{\mathbf{d}}^{\mathrm{T}}\widetilde{\mathbf{K}}\tilde{\mathbf{d}} = -\frac{1}{2}\tilde{\mathbf{d}}^{\mathrm{T}}\mathbf{f} = -\frac{1}{2}\mathbf{f}^{\mathrm{T}}\widetilde{\mathbf{K}}^{-1}\mathbf{f} = -\widetilde{U}(\tilde{\mathbf{d}}), \\ \hat{\Pi}(\hat{\mathbf{d}}) = \frac{1}{2}\hat{\mathbf{d}}^{\mathrm{T}}\widehat{\mathbf{K}}\hat{\mathbf{d}} - \hat{\mathbf{d}}^{\mathrm{T}}\mathbf{f} = -\frac{1}{2}\hat{\mathbf{d}}^{\mathrm{T}}\widehat{\mathbf{K}}\hat{\mathbf{d}} = -\frac{1}{2}\hat{\mathbf{d}}^{\mathrm{T}}\mathbf{f} = -\frac{1}{2}\mathbf{f}^{\mathrm{T}}\widehat{\mathbf{K}}^{-1}\mathbf{f} = -\widehat{U}(\hat{\mathbf{d}}). \end{cases} \tag{57}$$

The difference between the strain energies of FEM and PIM-LSS solution becomes

$$\widetilde{U}(\tilde{\mathbf{d}}) - \widehat{U}(\hat{\mathbf{d}}) = \frac{1}{2}\mathbf{f}^{\mathrm{T}}(\widetilde{\mathbf{K}}^{-1} - \widehat{\mathbf{K}}^{-1})\mathbf{f} \leqslant 0, \tag{58}$$

which gives

$$\widehat{U}(\hat{\mathbf{d}}) \geqslant \widetilde{U}(\tilde{\mathbf{d}}). \tag{59}$$

This completes the proof. Note that the above proof is similar to that given in [39]. □

Theorem 4 shows that the PIM-LSS will provide a more "softening" effect to system than FEM. In the following we examine some special models of PIM-LSS using different fitting orders.

When zero order fitting is used in Eq. (16), it is clear that $n = 1$, $\varphi_1 = 1$ and $\hat{\boldsymbol{\varepsilon}}$ is a constant in each nodal domain. Using Eq. (23) we can rewrite the strain $\hat{\boldsymbol{\varepsilon}}$ as

$$\int_{\Omega_k} \hat{\boldsymbol{\varepsilon}}\,\mathrm{d}\Omega = \int_{\Omega_k} \tilde{\boldsymbol{\varepsilon}}\,\mathrm{d}\Omega \tag{60}$$

or

$$\hat{\boldsymbol{\varepsilon}} = \frac{1}{A_k}\int_{\Omega_k} \tilde{\boldsymbol{\varepsilon}}\,\mathrm{d}\Omega, \tag{61}$$

which is exactly the same as that in NS-PIM, where A_k is the area of domain Ω_k.

Corollary 2. *The PIM-LSS with zero order fitting is exact the NS-PIM; and for any practical model with a reasonable number of elements, it will produce an upper bound solution in energy norm.*

The proof of Corollary 2 is similar to that in Ref. [39], and thus omitted.

On the other hand, Theorem 2 indicates that strain $\hat{\boldsymbol{\varepsilon}}$ will approach to the compatible strain $\tilde{\boldsymbol{\varepsilon}}$ when subspace W approaches to the space S. Therefore, there exist a proper order of fitting such that strain field $\hat{\boldsymbol{\varepsilon}}$ obtained using PIM-LSS approaches the compatible strain field $\tilde{\boldsymbol{\varepsilon}}$.

Corollary 3. *When finite order fittings are used, strain energy obtained using the PIM-LSS lies in between those of the compatible FEM model and the NS-PIM model when the same mesh is used. Furthermore, there exists a preferred order of fitting for strain field such that ultra-accurate solution can be obtained using the PIM-LSS.*

A preferred order of fitting for strain field is usually problem-dependent and also mesh-dependent. And hence it requires a number of trials-of-error to find that. Therefore, in real computation, we often use low order fittings, such as first order or second order polynomials models. The convergence and bound properties of these models will be examined in the following sections.

7. Numerical examples

In this section, a number of numerical examples will be examined using the PIM-LSS with both linear and quadratic displacement field. To investigate quantitatively the numerical results, the error indicators in both displacement and energy norms are defined as follows:

$$E_d = \sqrt{\frac{\sum_{i=1}^{n}(u_i^{\mathrm{ref}} - u_i^{\mathrm{num}})^2}{\sum_{i=1}^{n}(u_i^{\mathrm{ref}})^2}}, \tag{62}$$

$$E_e = \sqrt{\frac{|U_{\mathrm{num}} - U_{\mathrm{ref}}|}{U_{\mathrm{ref}}}} \tag{63}$$

where the superscript ref denotes the reference or analytical solution, num denotes a numerical solution obtained using a numerical method.

For the 2D problems, the following polynomial bases termed, respectively, as zero order, half-linear, linear, bilinear, quadratic fitting bases

$$\varphi_1 = 1, \tag{64}$$

$$\varphi_1 = 1, \quad \varphi_2 = xy, \tag{65}$$

$$\varphi_1 = 1, \quad \varphi_2 = x, \quad \varphi_3 = y, \tag{66}$$

$$\varphi_1 = 1, \quad \varphi_2 = x, \quad \varphi_3 = y, \quad \varphi_4 = xy, \tag{67}$$

$$\varphi_1 = 1, \quad \varphi_2 = x, \quad \varphi_3 = y, \quad \varphi_4 = xy, \quad \varphi_4 = x^2, \quad \varphi_4 = y^2 \tag{68}$$

are used to examine the convergence property of PIM-LSS. Note that we have total freedom to choose the basis functions for our strain field construction, as long as they are linearly independent. We need not worry about the completeness, which is on the hand known important in the displacement field construction [20,21].

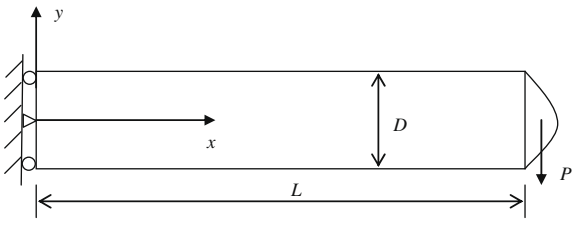

Fig. 4. A 2D cantilever solid subjected to a parabolic traction on the right edge.

7.1. Cantilever 2D solid

A 2D cantilever solid with length $L = 50$ m and height $D = 10$ m is now studied. The solid is subjected to a parabolic traction at the right end as shown in Fig. 4. The cantilever beam is studied as a plane stress problem with $E = 3.0 \times 10^7$ Pa, $P = -1000$ N and $\nu = 0.3$. Analytical solutions of this problem can be found in Ref. [45].

The displacement error of PIM-LSS with linear displacement field is first investigated and plotted in Fig. 5. When zero order model (64) and half-linear model (65) are used, the solutions from PIM-LSS have the almost-equal convergence rate and accuracy with linear FEM. However, when the higher order fittings are used, the convergent rates are respectively about 2.98 for linear fitting, 3.11 for bilinear fitting and 3.00 for quadratic fitting, which are much higher than the theoretical value of 2.0 for linear and bilinear FEM. Furthermore, higher convergent accuracy, which is 10 times more accurate than that of linear FEM, is also found for PIM-LSS using three higher order models.

Using Eq. (63), the energy error of PIM-LSS with linear displacement field is computed and plotted in Fig. 6. It is seen that the convergence rates in energy norm are, respectively, 1.6, 1.44 and 1.45 when linear, bilinear and quadratic polynomial bases are used, which is much higher than the theoretical value of 1.0 for linear and bilinear FEM. These examples show clearly the very high accuracy and excellent superconvergence of the PIM-LSS with higher order models.

The strain energy of PIM-LSS with linear displacement field is computed and plotted in Fig. 7. It is seen that PIM-LSS can produce the upper bound solution for zero order and half-linear fitting, and can produce lower bound solutions for the three higher order models. Furthermore, the strain energy from these models is in between those from the compatible FEM and the NS-PIM. In addition, it is found that the PIM-LSS solution approaches the FEM solution with an increase of order of fitting for reproduced strain. These findings verify the bound properties detailed in Section 6.

7.2. Infinite 2D solid with a circular hole

An infinite 2D solid with a central circular hole ($a = 1$ m) and subjected to a unidirectional tensile ($T_x = 10$ N/m) is studied. Owing to its two-fold symmetry, one quarter is modeled with $b = 5$ m (as shown in Fig. 8). Symmetry conditions are imposed on the left and bottom edges of the quarter model, and the inner boundary of the hole is traction free. For this benchmark problem, the analytical solution can be found in Ref. [45].

To study the convergence property of the PIM-LSS solution, the model with "nearly" regularly distributed nodes has been analyzed, and corresponding nodal distribution and background mesh is shown in Fig. 9. First, the strain energy of PIM-LSS with linear displacement field is computed and plotted in Fig. 10. It is see that PIM-LSS has upper and lower bounds solutions of the exact solution for different fitting orders. Furthermore, the strain energy for these models is in between that from the compatible FEM solu-

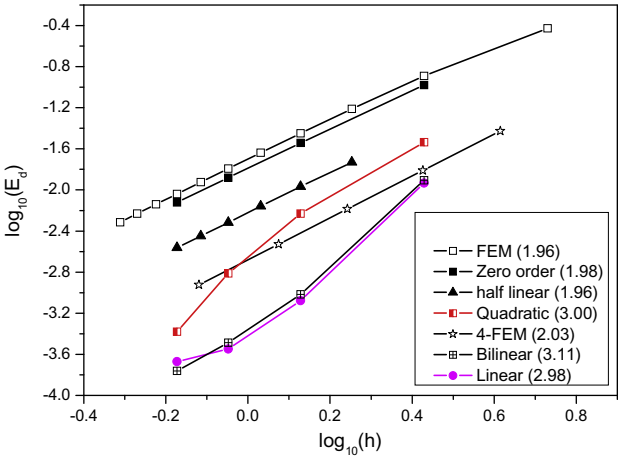

Fig. 5. Convergence of the PIM-LSS solution in displacement norm; it clearly shows very high accuracy and excellent superconvergence of the PIM-LSS with higher order models.

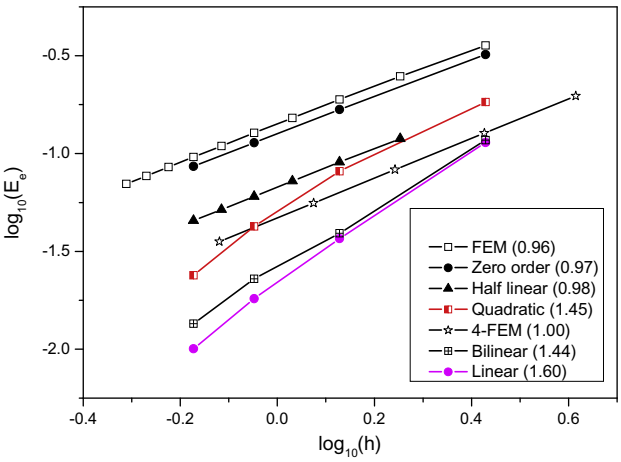

Fig. 6. Convergence of the PIM-LSS solution in energy norm; it clearly shows very high accuracy and excellent superconvergence the PIM-LSS with three higher order models.

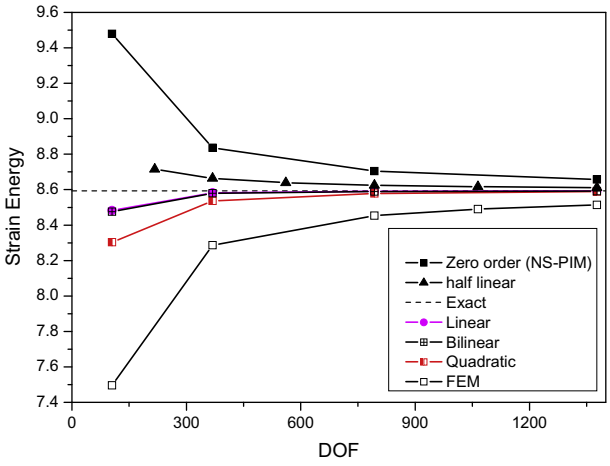

Fig. 7. Upper and lower bound solutions of the PIM-LSS for 2D beam.

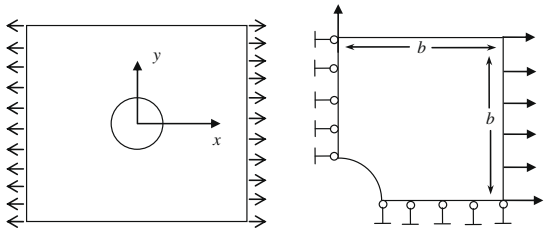

Fig. 8. Infinite 2D solid with a hole subjected to a tensile force and its quarter model.

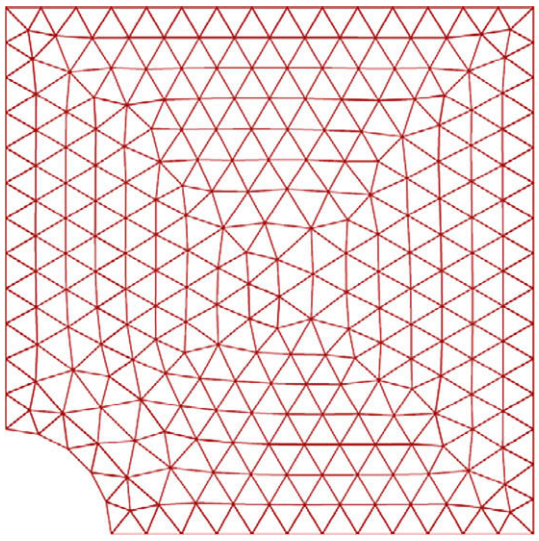

Fig. 9. Nodal distribution and background mesh for the quarter model of 2D solid with a hole.

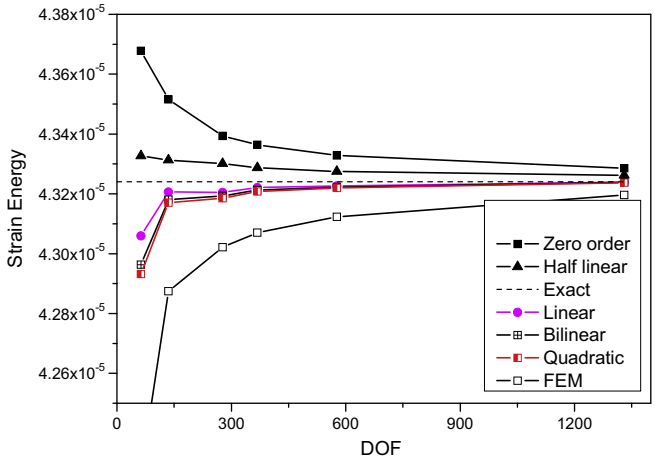

Fig. 10. Strain energy of the PIM-LSS for different fitting orders in a 2D solid with a hole.

tion and the NS-PIM solution. It also shows that the solution from PIM-LSS will approach the solution of FEM with an increase of orders of polynomial fitting. These findings verify again the bound properties of PIM-LSS.

Using Eqs. (62) and (63), errors in displacement and energy norms are computed and plotted against the average nodal spacing (h) as shown in Figs. 11 and 12. When linear, bilinear and quadratic fittings are used, the convergence rates for PIM-LSS in displacement norm are about 2.12, which is a litter higher than the theoretical value 2.0 of linear FEM. However, the convergent rates in energy norm are about 1.5 for three higher order models and obviously much higher than the theoretical value 1.0 of linear FEM.

We now test the convergence properties of PIM-LSS to the incompressible material. In this case, this infinite solid with a circular hole problem is studied as a plane strain problem, and the effects of Poisson's ratio on the convergence of PIM-LSS are examined. Fig. 13 plots the displacement error norm versus different Poisson's ration for the models of PIM-LSS. The results show that the PIM-LSS with zero order fitting avoids the volumetric locking naturally; while three higher order models are subjected to the volumetric locking. Furthermore, the more order models are used, the more sensitive is exhibited for PIM-LSS to the change of Poisson's ratio. Therefore, for the incompressible material, PIM-LSS with zero order fitting is a good candidate.

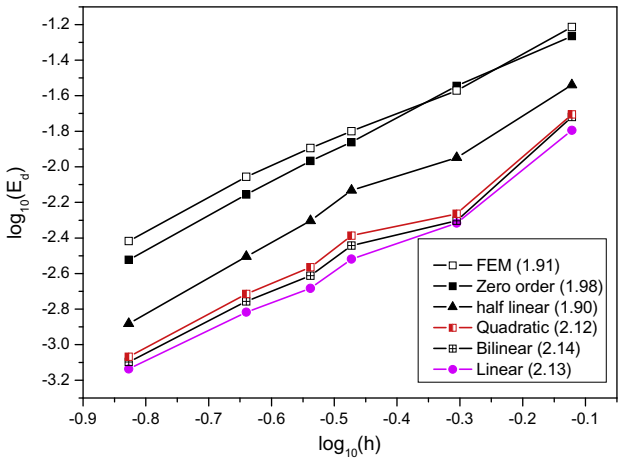

Fig. 11. Convergence of the PIM-LSS solution in displacement norm for infinite 2D solid with a circular hole.

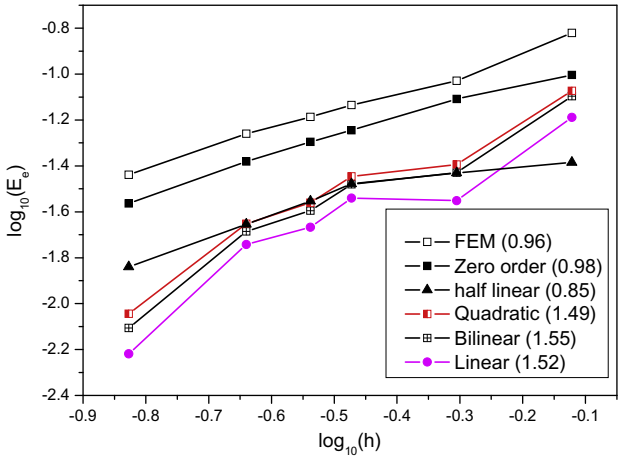

Fig. 12. Convergence of the PIM-LSS solution in energy norm for infinite 2D solid with a circular hole.

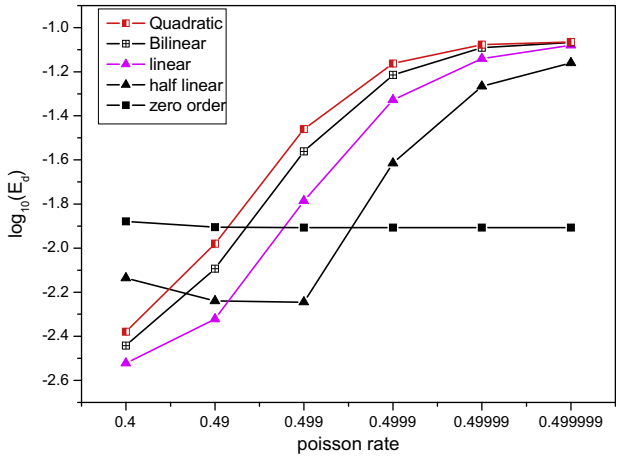

Fig. 13. Effects of Poisson's ration on the convergence properties of PIM-LS. It shows that PIM-LSS with zero order fitting can pass the volumetric locking, while other higher order models cannot.

Note that in the PIM-LSS, the strain obtained using least square is actually the average over the sub-domains sharing the same field node. Therefore, the nodal average of element stresses, which is usually used in the standard FEM, has actually been made and hence one does not need such post-processing procedure and avoids the extra computations of strain predictions and contour plotting of stresses. A comparison of contour plotting of stresses between FEM, NS-PIM and PIM-LSS with linear fitting is made in from Figs. 14–17, which shows that PIM-LSS produce the more accurate and more smoothed stresses solutions.

7.3. Semi-infinite plate

A two-dimensional half space subjected to a uniform pressure on the upper surface within a finite range ($-a \leqslant x \leqslant a$) is studied (see Fig. 18). Plane strain condition is considered and the analytical solutions can be found in Ref. [45]. Due to the symmetry about y-axis, the problem is modeled with a $5a \times 5a$ square with $a = 0.2$ m, $c = 100$ and $p = 1$ MPa. The left and bottom sides are constrained using exact displacement while the right side is subjected to tractions computed form the analytical solutions. The nodal distribution and background mesh of this model is shown in Fig. 19.

Fig. 20 shows the strain energy obtained using the PIM-LSS with linear displacement field for different strain fitting orders. It is clear that PIM-LSS has upper and lower bound solutions of the exact solution when the different fitting orders for strain construction are used. Furthermore, the strain energy for these models is no-less than that from the compatible FEM solution, and no-larger than the strain potential from the NS-PIM.

Using Eqs. (62) and (63), errors in displacement and energy norms are calculated and plotted in Figs. 21 and 22. It is seen that the convergence rate in displacement norm for the PIM-LSS is a little higher than that of the FEM solution. However, the convergence rate in energy norm is respectively about 1.57, 1.42, 1.34 for three higher order models, which is much higher than the theoretical value 1.0 of linear FEM. This clearly shows the superconvergence in energy norm.

7.4. Square solid subjected to uniform pressure and body force

A square solid is now studied as shown in Fig. 23. The solids are constrained on the left, the right, and the bottom edges, and suffering from uniform pressure along the top edge and body force of

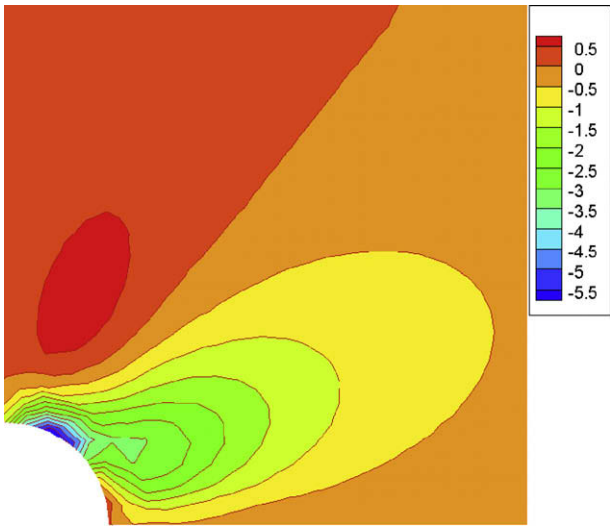

Fig. 14. Reference stresses solution σ_{xy} for the infinite 2D solid with hole.

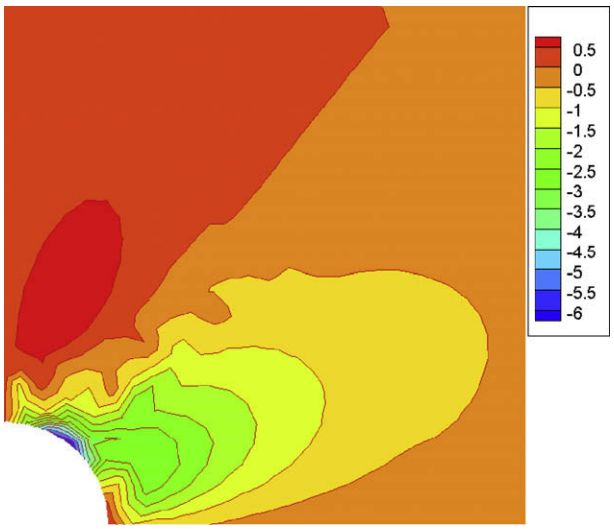

Fig. 15. Stress stresses solution σ_{xy} of linear FEM for the infinite 2D solid with hole.

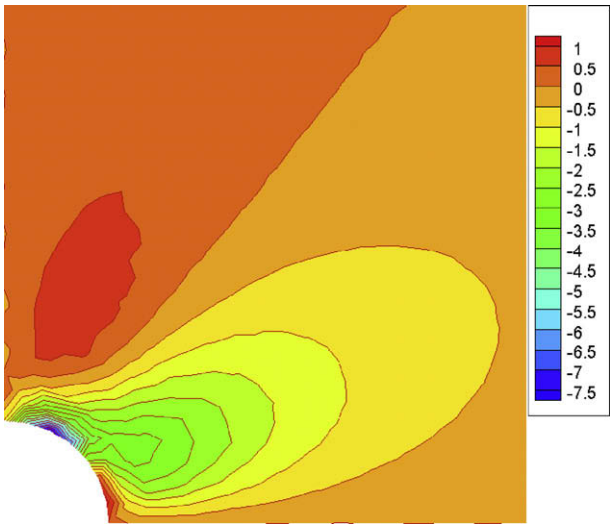

Fig. 16. Stress stresses solution σ_{xy} of NS-PIM for the infinite 2D with hole.

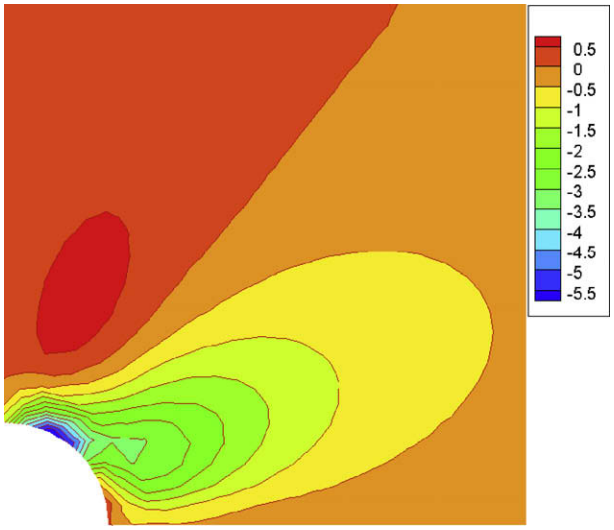

Fig. 17. Stress stresses solution σ_{xy} of PIM-LSS with linear fitting for the strain field.

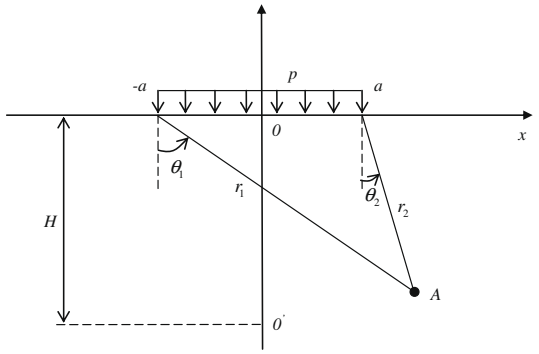

Fig. 18. Semi-infinite two-dimensional solid subjected to a uniform pressure on the surface.

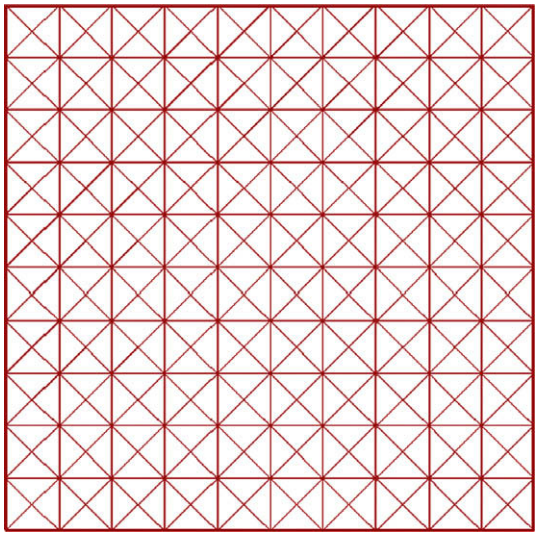

Fig. 19. Nodal distribution and background mesh for the semi-infinite two-dimensional solid.

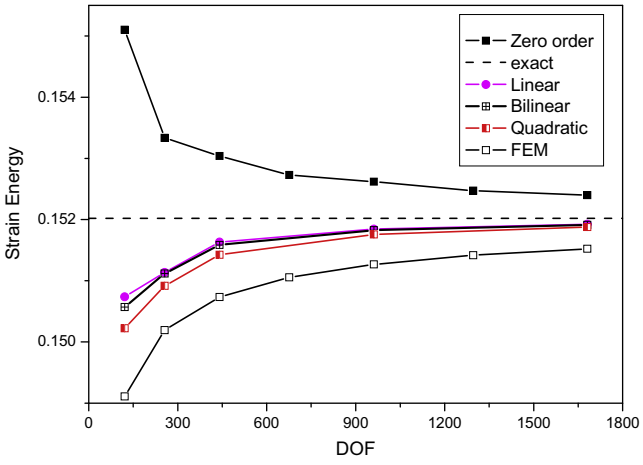

Fig. 20. Strain energy of the PIM-LSS for a two-dimensional half space subjected to a uniform pressure.

$\mathbf{b}^T = \{0, -1\}$. It is considered as plane stress problem with $\nu = 0.3$ and $E = 3.0 \times 10^7$ Pa.

The convergence property and energy bound for PIM-LSS with linear displacement field for different orders of strain fittings are also investigated in a similar way as in the previous examples. As

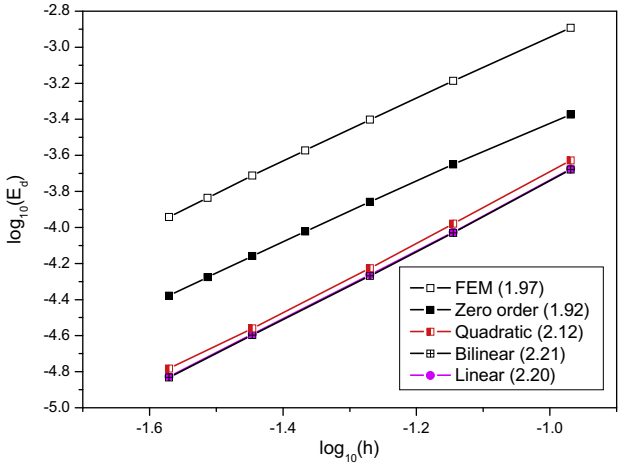

Fig. 21. Convergence of the PIM-LSS in displacement norm for a two-dimensional half space subjected to a uniform pressure.

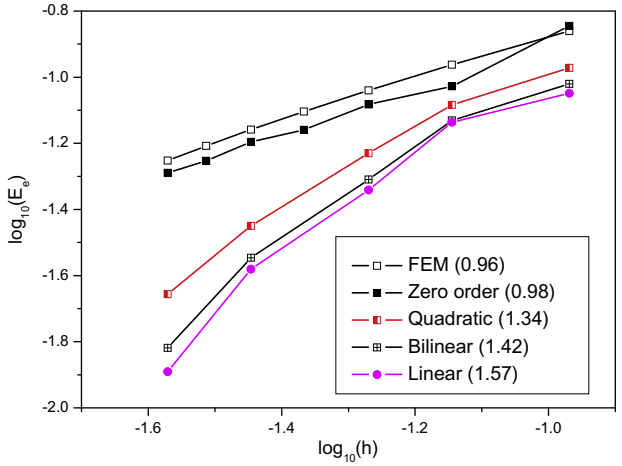

Fig. 22. Convergence of the PIM-LSS solution in energy norm for a two-dimensional half space subjected to a uniform pressure.

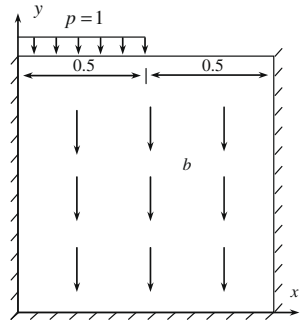

Fig. 23. A square solid with body force subjected to a uniform pressure.

the analytical solution is not available for this problem, the reference solution of strain energy is obtained using the FEM with a very fine mesh (8238 nodes). The computed strain energy and convergent rate in energy norm are plotted in Figs. 24 and 25, respectively. It is seen again that the linear PIM-LSS produces very high accurate solution in energy norm with a convergent rate of 1.22 for quadratic model and 1.24 for linear model, respectively.

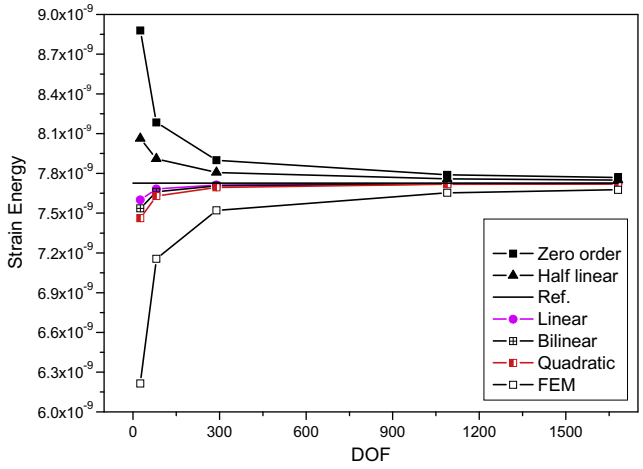

Fig. 24. Upper and lower bound solutions of the PIM-LSS for square solid subjected to uniform pressure and body force.

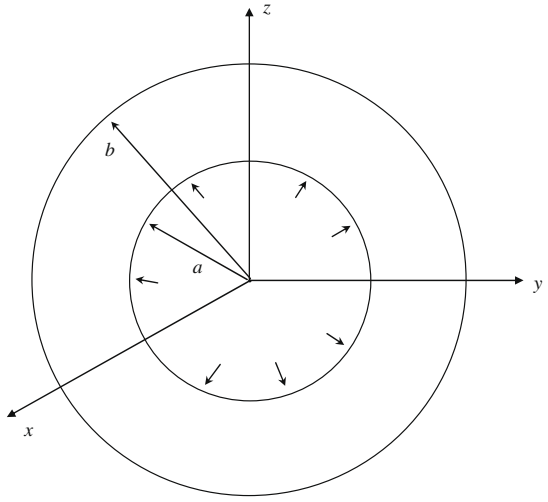

Fig. 26. The Lame problem of a hollow sphere under internal pressure.

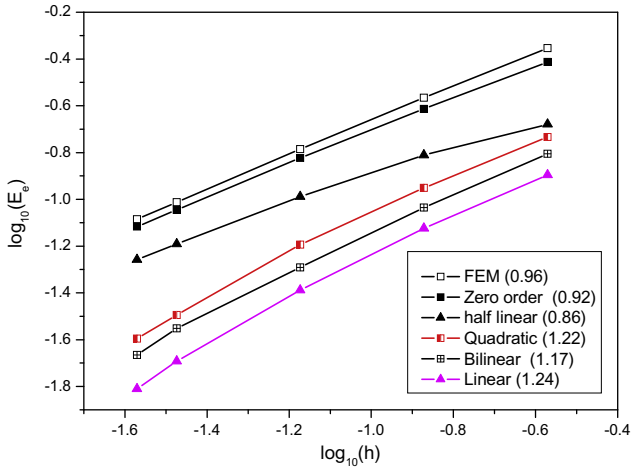

Fig. 25. Convergence of the PIM-LSS in energy norm for square solid subjected to uniform pressure and body force.

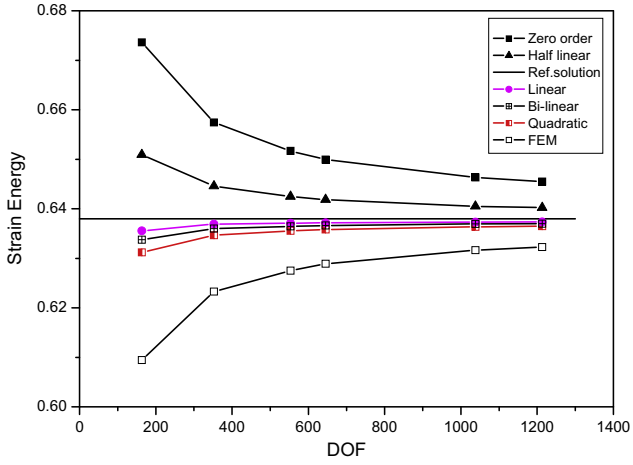

Fig. 27. Strain energy of the PIM-LSS with different fitting orders for the strain construction for 3D Lame problem. It shows that PIM-LSS can produce the upper and lower bound solutions and the strain energy from PIM-LSS is in that between from NS-PIM and FEM solution.

7.5. The 3D Lame problem

The 3D Lame problem consists of a hollow sphere with inner radius a and outer radius b and subjected to internal pressure P, as shown in Fig. 26. For this benchmark problem, the analytical solution is available in polar co-ordinate system [45]. As the problem is spherically symmetrical, only one-eighth of the sphere is modeled and symmetry conditions are imposed on the three planes of symmetry. The numerical solution of this problem has been calculated using the material parameters $E = 1.0$ kPa, $v = 0.3$, geometric parameters $a = 1$ m, $b = 2$ m and internal pressure $P = 1$ N/m^2.

To investigate the properties of convergence and efficiency of the present PIM-LSS, we compute the strain energy of PIM-LSS with linear displacement field for different orders of strain fittings as shown in Fig. 27. For comparison, the FEM using linear four-node tetrahedron element is also employed to study the problem with the same nodes distributions. It is clear that PIM-LSS has upper and lower bound solutions of the exact solution when the different fitting orders for strain construction are used. Furthermore, the strain energy for these models is no-less than that from the compatible FEM solution, and no-larger than the strain potential from the NS-PIM. In addition, the error in energy norm against the average nodal spacing of the nodes distribution (h) are plotted

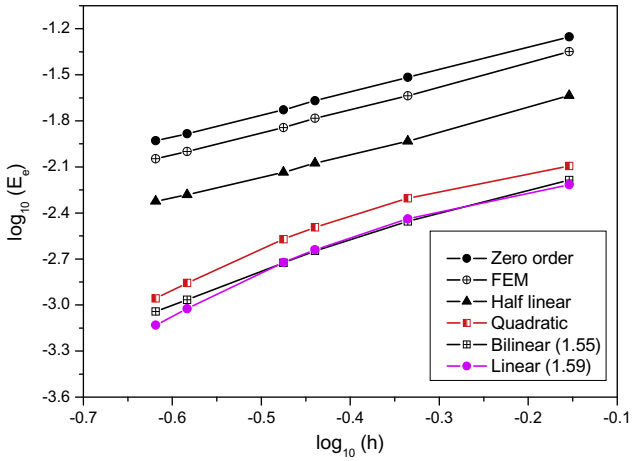

Fig. 28. Convergence of PIM-LSS solution in energy norm for different fitting orders used in the 3D Lame problem. It shows that the higher order fitting have better convergence properties.

in Fig. 28 for both the FEM and the four fitting models of PIM-LSS. It is found obviously that the higher order fitting for strain construction produces more accurate results, which are even about 10 times more accurate than that of linear FEM using the same nodal distributions.

7.6. PIM-LSS with high order polynomials interpolation

We now examine the 2D cantilever beam detailed in Section 7.1 using PIM-LSS with quadratic polynomials displacement field. A simple scheme [29] for local supporting node selection is adopted based on the background triangular cells for shape function construction. The background triangular cells are classified into two groups: interior cells and edge cells. An interior cell is a cell that has no edge on the boundary of the problem domain, and an edge cell is a cell that has at least one edge on the boundary of the problem domain. When the point of interest is located in an interior cell, we use six nodes for interpolation: three nodes located at the vertices of this cell, and the other three nodes located at the remote vertices of the three neighboring cells. The details on construction of quadratic PIM shape function based on triangular cells can be found in Ref. [29]. To study the convergence property of the PIM-LSS, the strain energy of PIM-LSS with quadratic displacement field for different fitting orders for strain construction is calculated in Fig. 29. It is clearly seen that PIM-LSS produces upper and lower bound solutions of the exact solution. Using Eqs. (62) and (63), errors in displacement and energy norms are calculated and plotted in Figs. 30 and 31. From these figures, it is observed that the very high accuracy and convergence rates in displacement norm and energy norm are obtained. This example shows clearly that the incompatible PIM shape functions can be used in our PIM-LSS model: a typical weakened weak (W^2) formulation [44].

Note that compared with the solutions using linear PIM shape functions, the solution using quadratic PIM shape functions are not necessarily better. This may be because of (1) the linear PIM performed already very good; (2) the smoothed strains are obtained using the Heaviside step smoothing function, which limits the order of accuracy.

7.7. Computational efficiency of PIM-LSS

Corollary 1 in Section 5 shows that the stiffness matrix obtained using PIM-LSS is symmetry, positive definite and has

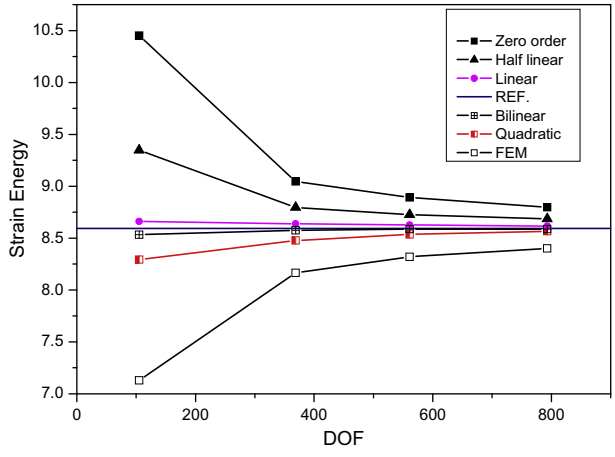

Fig. 29. Strain energy of the PIM-LSS with quadratic displacement field for 2D beam problem. This example shows that PIM-LSS can produce the upper and lower bound solutions and the strain energy from PIM-LSS is in that between from NS-PIM solution and FEM solution.

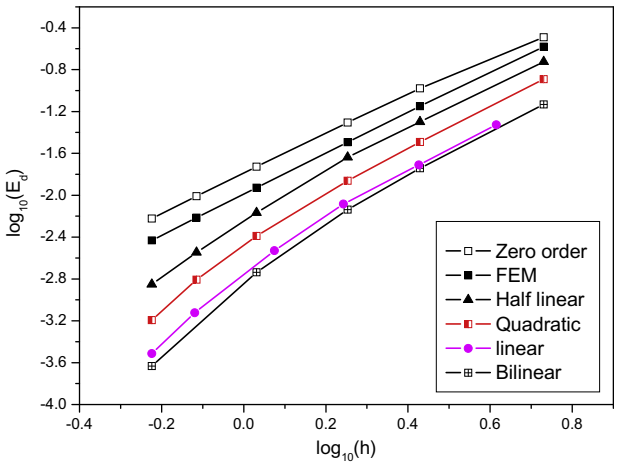

Fig. 30. Displacement error of the PIM-LSS solution with quadratic displacement field, it clearly shows very high accuracy and convergent rates of the PIM-LSS with higher order models.

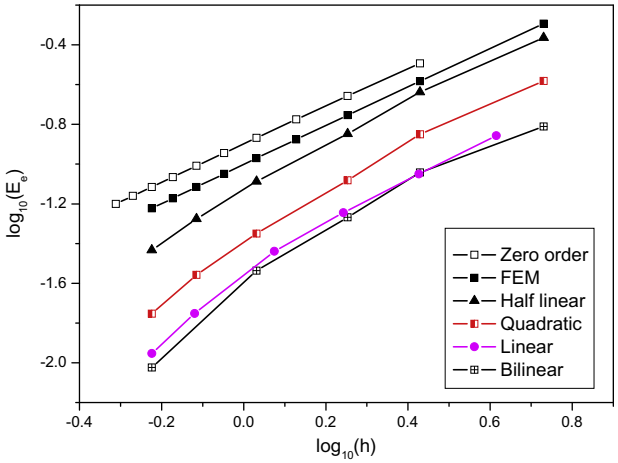

Fig. 31. Energy error of the PIM-LSS solution with quadratic displacement field, it clearly shows very high accuracy and convergent rates of the PIM-LSS with higher order models.

the same dimensions as that of FEM when the same mesh is used. This is because PIM-LSS has not introduced any extra unknown variables compared to the FEM. Considering the extra computing cost in computing the strain field for establishing the stiffness matrix, PIM-LSS will take more computation time compared to the FEM. However, when an iterative solver is used, the PIM-LSS equations can be solved more efficiently because of the better conditioning in stiffness matrix due to the softening effects. Furthermore, the much higher accuracy and convergence of PIM-LSS will result in a higher computational efficiency compared to the FEM.

For a fairer comparison, we now produce the efficient curve: CPU time taken for the solution with same accuracy. Figs. 32 and 33 plot respectively the energy and displacement errors against the CPU times used by FEM and PIM-LSS with different fitting orders. In this comparison, full matrix solver is used. It is clear that for the same CPU time PIM-LSS with linear and bilinear fitting can obtain solution of higher accuracy; and for the same accuracy in solution PIM-LSS for linear and bilinear fitting needs less CPU times than that from FEM. Therefore, the PIM-LSS with the linear and bilinear fitting has more efficient than that the FEM models with the same nodal distributions.

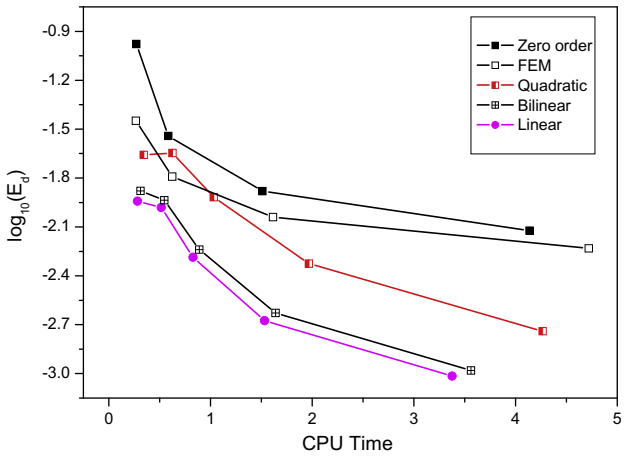

Fig. 32. Comparisons of efficiency between FEM and PIM-LSS in displacement norm.

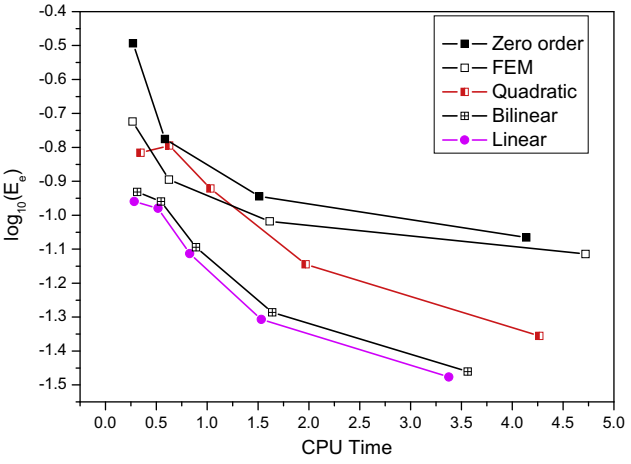

Fig. 33. Comparisons of computational efficiency between FEM and PIM-LSS in energy norm.

7.8. Discussion on PIM-LSS

Note that the least square techniques have been often used in formulating meshfree methods [21] and other numerical methods such as the "least square point interpolation method" formulated in Refs. [46,47]. In these methods, the least square technique is used to approximate the displacement fields. In the present PIM-LSS, however, the least square fitting technique is used to construct *stain* field. This may be one of the distinct features of the present PIM-LSS.

In this paper, the polynomial PIM shape functions are used for establishing the assumed displacement field. Other types of shape functions such as the RPIM shape functions [16,33,48] and the Kriging formulation [17–19,49] can also be used for the displacement filed assumption. The incompatibility of these shape functions will not affect the stability and the convergence of the PIM-LSS. Note that the RPIM and the Kriging are essentially the same as proven in [18].

In the present PIM-LSS, the least square technique is used to construct the strain field in each nodal domain. This is different from the "assumed strain" methods such as the "quasi-conforming technique" [50]. First, our PIM-LSS is basically still an "assumed displacement" or displacement methods, because the only unknown field in the PIM-LSS is the displacement field, and the construction of the strain field is entirely depends on the assumed displacement field. Second, our strain field construction is based on nodal domains not on elements. We use meshes in an intertwined fashion: displacement field assumption is based on cells/elements, and strain field construction is based on nodes: a typical W^2 formulation [44]. Third, our PIM-LSS works very well for triangular mesh, due largely to the intertwined cells/domain structure that offers the important softness to the model [22,44]. Forth, PIM-LSS does not introduce any addition degrees of freedoms in any way.

8. Conclusions

In this work, we develop a least square point interpolation method (PIM-LSS), where the PIM shape functions are used to construct the assumed displacement field and the least square technique for strain field construction based on the assumed displacement field. The PIM-LSS can construct strain fields of desired order including the zero-order approximation used in the NS-PIM, and therefore can be considered as a high order extension of the NS-PIM with more general foundation of projection theory. We proved theoretically: (1) The PIM-LSS is variational consistent, stable and hence convergent. (2) When the same mesh is used the strain energy obtained using the PIM-LSS is in between those from the compatible FEM and the NS-PIM models. (3) The exact solution can usually be bounded by the PIM-LSS solutions with strain field of both lower order and higher order fittings. (4) There exists a proper order polynomial fitting such that the PIM-LSS produce the ultra-accurate solutions. (5) The PIM-LSS works very well with triangular mesh. Intensive numerical studies have verified the theorems, convergence, bounds property of strain energy, and ultra-accuracy of the PIM-LSS.

Acknowledgements

This work was supported in part by the National Natural Science Foundation of China under Grants 10532050, 10501017, 60673023, and by the 985 program of Jilin University, China. The authors also thank to the support of Centre for ACES and Singapore-MIT Alliance (SMA), National University of Singapore.

References

[1] O.C. Zienkiewicz, R.L. Taylor, The Finite Element Method, fifth ed., Butterworth Heinemann, Oxford, UK, 2000.
[2] G.R. Liu, S.S. Quek, The finite Element Method: A Practical Course, Butterworth Heinemann, Oxford, 2003.
[3] S.C. Brenner, L.R. Scott, The Mathematical Theory of Finite Element Methods, Spring-Verlag, 1994.
[4] B. Dietrich, Finite Elements: Theory, Fast Solvers, and Applications in Solid Mechanics, Cambridge University Press, 2007.
[5] A.A. Samarskiĭ, P.N. Vabishchevich, L.G. Vulkov, Finite Difference Methods: Theory and Applications, Nova Science Publishers, New York, 1999.
[6] G.E. Forsythe, W.R. Wasow, Finite-Difference Methods for Partial Differential Equations, Cambridge University Press, Wiley, New York, 1960.
[7] R.J. LeVeque, Finite Volume Methods for Hyperbolic Problems, Cambridge University Press, New York, 2002.
[8] R.H. Li, Z.Y. Chen, W. Wu, Generalized Difference Methods for Differential Equations: Numerical Analysis of Finite Volume Methods, Marcel Dekker, New York, 2000.
[9] L.B. Lucy, A numerical approach to testing the fission hypothesis, The Astron. J. 8 (1977) 1013–1024.
[10] G.R. Liu, M.B. Liu, Smoothed Particle Hydrodynamics—A Meshfree Practical Method, World Scientific, Singapore, 2003.
[11] B. Nayroles, G. Touzot, P. Villon, Generalizing the finite element method: diffuse approximation and diffuse elements, Comput. Mech. 10 (1992) 307–318.
[12] T. Belytschko, Y.Y. Lu, L. Gu, Element-free Galerkin methods, Int. J. Numer. Methods Engrg. 37 (1994) 229–256.
[13] W.K. Liu, S. Jun, Y.F. Zhang, Reproducing kernel particle methods, Int. J. Numer. Methods Engrg. 20 (1995) 1081–1106.
[14] S.N. Atluri, T. Zhu, A new meshless local Petrov–Galerkin (MLPG) approach in computational mechanics, Comput. Mech. 22 (1998) 117–127.

[15] G.R. Liu, Y.T. Gu, A point interpolation method for two-dimensional solids, Int. J. Numer. Methods Engrg. 50 (2001) 937–951.
[16] J.G. Wang, G.R. Liu, A point interpolation meshless method based on radial basis functions, Int. J. Numer. Methods Engrg. 54 (2002) 1623–1648.
[17] L. Gu, Moving Kriging interpolation and element-free Galerkin method, Int. J. Numer. Methods Engrg. 56 (2003) 1–11.
[18] K.Y. Dai, G.R. Liu, K.M. Lim, Y.T. Gu, Comparison between the radial point interpolation and the Kriging based interpolation using in meshfree methods, Comput. Mech. 32 (2003) 60–70.
[19] P. Tongsuk, W. Kanok-Nukulchai, Further investigation of element-free Galerkin method using moving Kriging interpolation, Int. J. Comput. Methods 1 (2004) 345–365.
[20] G.R. Liu, Meshfree Methods: Moving Beyond the Finite Element Method, CRC Press, Boca Raton, USA, 2002.
[21] G.R. Liu, Y.T. Gu, An Introduction to Meshfree Methods and their Programming, Springer, Dordrecht, the Netherlands, 2005.
[22] G.R. Liu, A generalized gradient smoothing technique and the smoothed bilinear form for Galerkin formulation of a wide class of computational methods, Int. J. Comput. Methods 5 (2008) 199–236.
[23] B. Brezzi, M. Michel, Mixed and Hybrid Finite Element Method, Spring, New York, 1991.
[24] J.C. Simo, T.J.R. Hughes, Computational Inelasticity, Sprint, New York, 1998.
[25] T.H.H. Pian, C.C. Wu, Hybrid and Incompatible Finite Element Methods, CRC Press, Boca Raton, FL, 2006.
[26] J.S. Chen, C.T. Wu, S. Yoon, Y. You, A stabilized conforming nodal integration for Galerkin mesh-free methods, Int. J. Numer. Methods Engrg. 50 (2001) 435–466.
[27] G.R. Liu, K.Y. Dai, T.T. Nguyen, A smoothed element method for mechanics problems, Comput. Mech. 39 (2007) 859–877.
[28] G.R. Liu, T.T. Nguyen, K.Y. Dai, K.Y. Lam, Theoretical aspects of the smoothed finite element method (SFEM), Int. J. Numer. Methods Engrg. 71 (2007) 902–930.
[29] G.R. Liu, G.Y. Zhang, K.Y. Dai, Y.Y. Wang, Z.H. Zhong, G.Y. Li, X. Han, A linearly conforming point interpolation method (NS-PIM) for 2D solid mechanics problems, Int. J. Comput. Methods 2 (2005) 645–665.
[30] G.R. Liu, T.T. Nguyen, X.H. Nguyen, K.Y. Lam, An edge-based smoothed finite element method (E-SFEM) for static, free and forced vibration analysis, J. Sound Vib., 2007, revised.
[31] G.Y. Zhang, G.R. Liu, Y.Y. Wang, H.T. Huang, Z.H. Zhong, G.Y. Li, X. Han, A linearly conforming point interpolation method (NS-PIM) for three-dimensional elasticity problems, Int. J. Numer. Methods Engrg. 72 (2007) 1524–1543.
[32] Y. Li, G.R. Liu, M.T. Luan, K.Y. Dai, Z.H. Zhong, G.Y. Li, X. Han, Contact analysis for solids based on linearly conforming radial point interpolation method, Comput. Mech. 39 (2007) 859–877.
[33] G.R. Liu, Y. Li, K.Y. Dai, M.Y. Luan, W. Xue, A linearly conforming RPIM for 2D solid mechanics, Int. J. Comput. Methods 3 (2006) 401–428.
[34] S.C. Wu, G.R. Liu, H.O. Zhang, G.Y. Zhang, A node-based smoothed point interpolation method (NS-PIM) for thermoelastic problems with solution bounds, Int. J. Heat and Mass Trans. 52 (2009) 1464–1471.
[35] G.R. Liu, K. Zaw, Y.Y. Wang, Rapid inverse parameter estimation using reduced-basis approximation with asymptotic error estimation, Comput. Methods Appl. Mech. Engrg. 197 (2008) 3898–3910.
[36] G.R. Liu, K. Zaw, Y.Y. Wang, B. Deng, A novel reduced-basis method with upper and lower bounds for real-time computation of linear elasticity problems, Comput. Methods Appl. Mech. Engrg. 198 (2008) 269–279.
[37] G.R. Liu, X. Xu, G.Y. Zhang, T.T. Nguyen, A superconvergent point interpolation method (SC-PIM) with piecewise linear strain field using triangular mesh, Int. J. Numer. Method Engrg. (2008), doi:10.1002/nme.2464.
[38] G.R. Liu, X. Xu, G.Y. Zhang, Y.T. Gu, A point interpolation method with continuous strain field and superconvergence (PIM-CS) based on triangular mesh, Comput. Mech. (2008), doi:10.1007/s00466-008-0336-5.
[39] G.R. Liu, G.Y. Zhang, Upper bound solution to elasticity problems: a unique property of the linearly conforming point interpolation method (NS-PIM), Int. J. Numer. Methods Engrg. 74 (2008) 1128–1161.
[40] A.G. Arthur, M.H. Frank, Least Square Estimation with Application to Digital Signal Processing, John Willey & Sons, Inc., 1985.
[41] L. Peter, S. Kestutis, Curve and Surface Fitting an Introduction, Academic Press, 1986.
[42] G.L. David, Optimization by Vector Space Methods, John Wiley & Sons, Inc., 1969.
[43] J.C. Simo, T.J.R. Hughes, On the variational foundations of assumed strain methods, J. Appl. Mech. 53 (1986) 51–54.
[44] G.R. Liu, A weakened weak (W2) form for a unified formulation of compatible and incompatible methods, Part I. Theory and Part II. Application to solid mechanics problems, Int. J. Numer. Methods Engrg., revised.
[45] S.P. Timoshenko, J.N. Goodier, Theory of Elasticity, third ed., McGraw, New York, 1970.
[46] B.R. Zhang, R. Rajendran, 'FE-Eshfree' Quad4 element for free-vibration analysis, Comput. Method Appl. Mech. Engrg. 197 (2008) 3595–3604.
[47] R. Rajendran, B.R. Zhang, A 'FE-Eshfree' QUAD4 element based on partition of unity, Comput. Method Appl. Mech. Engrg. 197 (2007) 128–147.
[48] J.G. Wang, G.R. Liu, On the optimal shape parameters of radial basis functions used for 2-D meshless methods, Comput. Methods Appl. Mech. Engrg. 191 (2002) 2611–2630.
[49] P. Plengkhom, W. Kanok-Nukulchai, An enhancement of finite element method with moving Kriging shape functions, Int. J. Comput. Methods 2 (2005) 451–477.
[50] L.M. Tang, W.J. Chen, Y.X. Liu, String net approximation and quasi-conforming technique, in: S.N. Atluri, R.H. Gallagher, Zienkiewicz (Eds.), Hybrid and Mixed Finite Element Methods, Wiley, Chichester, 1983, pp. 173–188.